Article:

Aburziza, A.A., Naderi, M. and Gladwin, D.T. (2026) A detailed analysis of long-term modelling method of power-to-gas hydrogen generation using curtailed wind energy. Energies, 19 (9). 2232. ISSN: 1996-1073

https://doi.org/10.3390/en19092232

energies

MDPI

Article

A Detailed Analysis of Long-Term Modelling Method of Power-to-Gas Hydrogen Generation Using Curtailed Wind Energy

Abdussalam A. Aburziza *, Mobin Naderi and Daniel T. Gladwin

School of Electrical and Electronic Engineering, The University of Sheffield, Western Bank, Sheffield S10 2TN, UK; mobin.naderi@sheffield.ac.uk (M.N.); d.gladwin@sheffield.ac.uk (D.T.G.)
* Correspondence: aaaburziza1@sheffield.ac.uk

Abstract

Wind curtailment in Great Britain (GB) is increasing, leading to underutilisation of low-carbon energy and higher system costs. This paper develops a data-driven techno-economic framework for a hydrogen generation and storage system that converts curtailed wind energy into hydrogen. By modelling curtailment time series and electricity prices, and considering a proton exchange membrane (PEM) electrolyser-based power-to-gas system, The framework explicitly represents the operation and interaction of the PEM electrolyser, hydrogen compression, and high-pressure storage under time-varying curtailment and electricity price conditions using reconstructed GB curtailment time series. The levelised cost of hydrogen (LCOH), net present value (NPV), and delivered hydrogen volumes are evaluated. A new sizing metric, curtailment utilisation, is introduced to link curtailment availability with electrolyser and storage productivity. Using a GB curtailment dataset, two key relationships are identified. First, increasing access to low-cost curtailed energy reduces the LCOH until electrolyser utilisation saturates, beyond which additional energy purchases provide diminishing benefits. Second, hydrogen storage exhibits an economic optimum: Undersized tanks increase costs due to ramping and venting losses, whereas oversized tanks raise capital investment requirements and increase the LCOH. For the best-performing configuration, corresponding to 70.2 MWh of curtailed energy, a 2.3 MW electrolyser, and a 94 m^3 high-pressure tank, the system achieves an LCOH of £3.51/kg H_2 (excluding downstream delivery) and an NPV of £2.17 M and meets 98.01% of the hydrogen demand. These results indicate that optimal system design requires not only appropriate component sizing but also explicit consideration of curtailment profiles and pricing structures. The proposed framework provides decision-grade guidance for developers and policymakers evaluating hydrogen production from wind curtailment. Future work will extend the model to hybridise with other energy storage system technologies, enable revenue stacking across multiple markets, address real-gas storage modelling, examine the sensitivity of stack degradation, and incorporate transport and delivery costs. These findings show that viable hydrogen production from curtailed wind depends on both low-cost electricity and coordinated electrolyser storage sizing under realistic curtailment conditions. The framework provides practical guidance for developers and policymakers.

Keywords: hydrogen production; storage system; curtailed wind energy; power-to-gas; techno-economic analysis

Check for updates

Academic Editor: Benjamin McLellan

Received: 28 March 2026
Revised: 20 April 2026
Accepted: 29 April 2026
Published: 5 May 2026

1. Introduction

The rapid growth of distributed energy systems has accelerated the integration of locally available renewable energy sources (RES), particularly wind and solar power [1]. However, the inherent variability and intermittency of RES pose persistent challenges for maintaining system reliability and balancing electricity supply and demand. Because renewable generation cannot be dispatched on demand, periods of excess electricity production frequently arise, during which surplus energy is curtailed or wasted rather than stored or utilised. In GB, wind generation reached approximately 83 TWh in 2024, yet around 10% (8.3 TWh) was curtailed due to transmission constraints, network congestion, and insufficient storage infrastructure [2,3]. This issue is particularly pronounced for wind energy, which exhibits variability across hourly, daily, and seasonal timescales [4]. Effectively managing these fluctuations, therefore, requires advanced energy storage solutions capable of absorbing excess generation and either returning it to the grid at a later time or converting it into alternative energy carriers.

Energy storage system (ESS) technologies play a critical role in mitigating RES variability and enhancing grid flexibility and stability [5]. Different storage technologies provide distinct services depending on their power, energy, and duration characteristics. Battery energy storage systems (BESS) are widely deployed for short-term balancing and ancillary services but are constrained by limited energy capacity, relatively high costs, and self-discharge losses [6]. Pumped-hydro storage remains the most mature large-scale, long-duration storage technology, yet its deployment is geographically constrained and often hindered by environmental and permitting challenges [7]. Other options, such as compressed air energy storage and thermal energy storage, have been proposed but currently face limitations in efficiency, or site availability for seasonal applications [8].

Among these alternatives, power-to-gas (P2G) technology has attracted growing attention due to its potential to convert surplus renewable electricity into hydrogen, which can be stored over long periods with minimal loss, transported, and utilised across multiple sectors [9,10]. In contrast to electrochemical batteries, hydrogen storage offers a viable pathway for monthly-to-seasonal energy storage, despite lower round-trip efficiencies. Importantly, P2G enables the direct utilisation of curtailed wind energy (CWE) by converting otherwise wasted electricity into a valuable energy commodity via electrolysis [11].

Literature Review

In recent years, the utilisation of curtailed renewable energy for hydrogen production has attracted renewed attention, driven by increasing curtailment volumes, declining electrolyser costs, and the emergence of hydrogen markets. Several published studies have moved beyond early conceptual analyses and investigated data-driven, system-level approaches for integrating hydrogen into renewable-dominated power systems. Operationally focused studies have examined the short-term use of curtailed wind through flexible assets. Biggins and Brown [12] developed an optimisation framework to evaluate the economic performance of onshore wind co-located with battery storage and a hydrogen electrolyser under curtailment conditions in GB. Wind curtailment was represented probabilistically using a Markov chain calibrated to historical data, and the optimisation maximised short-term profit through coordinated scheduling of batteries and hydrogen production. While the results showed that hydrogen electrolysers are more effective than batteries in absorbing curtailed wind, the analysis was limited to operational scheduling over a short time horizon. It did not address long-term system planning, hydrogen storage sizing, or planning-oriented economic trade-offs.

At a broader system level, Yan et al. [13] developed a mixed-integer linear optimisation framework for coupling wind electricity, hydrogen production, and natural gas networks.

https://doi.org/10.3390/en19092232

Using real curtailed wind electricity data, the study demonstrated that hydrogen blending into gas pipelines can accommodate a portion of curtailed wind energy under infrastructure constraints. However, the focus was on network-level coupling and the feasibility of hydrogen blending, rather than on electrolyser utilisation efficiency, hydrogen storage sizing, or the long-term economics of hydrogen generation and storage systems. The authors in [14] carried out an extensive sensitivity analysis using multiple technical and economic indicators across a range of solar, wind, battery, and electrolyser configurations. However, some of the selected variable parameters and their assumed ranges appear to be of limited practical relevance, such as an electrolyser efficiency range extending from 60% to 100%.

Other studies have advanced the techno-economic modelling of wind-to-hydrogen systems without explicitly focusing on curtailment. Rezaei et al. [15] conducted a detailed techno-economic assessment of offshore wind-based hydrogen production, incorporating dynamic PEM electrolyser operation and high-resolution meteorological wind modelling. Their results highlighted the benefits of dynamic operation and economies of scale in reducing hydrogen production costs. Nevertheless, wind electricity was assumed to be fully dedicated to hydrogen production, and grid-driven curtailment, congestion constraints, and curtailed energy pricing were not modelled. In [16], a detailed MATLAB/Simulink-based model is developed for sizing renewable-energy and hydrogen-storage components for green hydrogen production; however, the analysis is limited to a specific hydropower–solar case study, and sizing decisions are derived from graphical assessment of performance metrics rather than through a formal optimisation procedure.

Several studies have explicitly linked hydrogen production to curtailed renewable electricity, but they have employed simplified planning assumptions. Park et al. [17] analysed green hydrogen production from curtailed wind and solar power using meteorological data and defined curtailment as residual generation after fixed grid export limits. Similarly, Abadie and Chamorro [18] investigated wind-based hydrogen production from an investor's perspective under economic and physical uncertainty, allowing an assumed unused share of wind generation to be allocated to hydrogen production. Although these studies offered useful insights, they did not explicitly model curtailment as a time-series process, nor did they provide a detailed treatment of hydrogen storage sizing in planning-oriented assessments.

Ferguson et al. [19] examined the integration of wind and tidal energy for hydrogen production in Orkney, GB. Their techno-economic analysis showed that hydrogen production becomes cost-effective when supplemented with grid electricity; however, reliance on tidal energy increased production costs due to higher electricity prices, while wind-only operation required substantial hydrogen storage capacity to manage variability. More recently, Niaz et al. [20] investigated the utilisation of curtailed renewable energy using battery energy storage systems and hydrogen production in a profit-maximisation framework. Zhao et al. [21] conducted a life-cycle cost analysis of the BIG HIT project, incorporating a feed-in tariff for curtailed wind energy. These studies further demonstrated the promise of hydrogen for curtailment mitigation, but they did not explicitly examine the interaction between curtailment variability, electrolyser utilisation, and hydrogen storage sizing.

Recent studies have increasingly examined hydrogen production from surplus and curtailed renewable electricity, reflecting the growing scale and practical importance of wind curtailment. Nevertheless, several important gaps remain in the existing literature. First, curtailed wind energy is frequently represented using assumed, aggregated, or probabilistic inputs rather than reconstructed time-series data with associated pricing information, which limits the ability to capture its temporal variability and economic implications. Second, electrolyser and hydrogen storage sizing are often treated as fixed or scenario-based decisions, rather than being explicitly linked to curtailed wind availability, utilisation efficiency, and storage saturation behaviour. Third, many published studies focus either on short-term operation or high-level techno-economic valuation, with limited attention to long-term planning trade-offs under constrained curtailed wind availability.

To address these gaps, this paper develops a data-driven long-term planning framework for hydrogen generation and storage using curtailed wind energy in Great Britain. As summarised in Tables 1 and 2, the main contributions of this study relative to the selected literature are as follows:

- A reproducible approach is developed to reconstruct hourly curtailed wind energy from aggregated curtailment records, allowing time-resolved curtailed wind inputs to be incorporated into long-term hydrogen system planning when site-specific high-resolution data are unavailable.
- A detailed hourly hydrogen generation and storage system model is established, linking curtailed wind input, electrolyser behaviour, hydrogen mass flow, storage tank dynamics, and operational control constraints within a unified planning framework.
- The study explicitly examines the relationship between curtailed wind energy utilisation and hydrogen storage sizing, and identifies the distinction between curtailment utilisation saturation and the economically optimal storage range.
- An integrated techno-economic assessment is carried out using real GB curtailment data and electricity pricing assumptions to evaluate hydrogen delivery capability, system operation, LCOH, NPV, and discounted payback period under long-term planning conditions.

The rest of the paper is organised as follows. Section 2 outlines the techno-economic modelling framework for the hydrogen generation and storage system (HGSS) and the sensitivity-analysis-based planning approach. Section 3 presents the simulation results and discussion. Section 4 outlines the main limitations and future work. Finally, Section 5 summarises the study's key findings and conclusions.

https://doi.org/10.3390/en19092232

Table 1. Comparison of recent studies on hydrogen utilisation of curtailed wind energy.

Ref.	Main Idea	Sizing Method	Modelling Method	Level of Modelling Detail	Metrics Used	Resolution of CWE	Limitation Addressed in This Study
[12]	Profit-maximising curtailed wind with BESS	Optimisation-based	Short-term optimisation-based scheduling	Medium (operation)	Medium operation, limited planning detail	Half-hourly (Markov chain)	Long-term modelling, storage sizing
[13]	Wind H_2 natural gas system coupling	MILP-based optimisation	Network-level energy system optimisation	High (network-level)	System cost	Hourly	H_2 storage sizing
[14]	SA for solar and wind H_2 production	Multi-objective SA	Techno-economic simulation	Medium	LCOH, LOCE, H_2 output	Seconds	Real curtailment, storage sizing
[15]	Dynamic offshore wind H_2 production	Scenario-based scaling	Dynamic component-level techno-economic simulation	High (component-level)	LCOH, H_2 output	Seconds	Real curtailment, storage sizing
[16]	Curtailment of hydro power	Multi-objective SA	Techno-economic modelling	Low (system-level)	Income, H_2 generation	Hourly	Lack of optimisation
[17]	Curtailment-mitigating H_2 production	CF-based sizing	Weather-driven techno-economic modelling	Medium (system-level)	LCOH, CF	Hourly	Real curtailment, storage sizing
[18]	Uncertain wind-based H_2 valuation	NPV-max capacity	Economic Monte Carlo valuation	Low–medium (economic)	NPV focus	Averaged	Real curtailment modelling, storage sizing
[19]	Hybrid wind–tidal	Scenario-based sizing	Integrated techno-economic assessment	Medium	LCOH, H_2 cost	No curtailment	Real curtailment, storage sizing
[20]	Profit-maximising curtailed RES	Optimisation-based sizing	Short-term optimisation-based dispatch	Medium	Profit, payback period	Hourly	Long-term H_2 planning
[21]	Wind-to-H_2 life-cycle cost assessment	Fixed-scale sizing	Life-cycle cost analysis	Low–medium	LCOH, life-cycle cost	Averaged	Real curtailment
This study	Curtailed wind-to-H_2 with constrained storage control	Scenario-based constrained sizing	Rule-based supervisory control with physical constraints	High (component-level)	LCOH, utilisation, storage performance	Hourly	Addresses long-term operation, real curtailment reconstruction, and H_2 storage sizing

https://doi.org/10.3390/en19092232

Table 2. Comparison of the main contributions of this study with selected previous studies.

Modelling Feature	[12]	[18]	[16]	[14]	[13]	[15]	This Work
Hourly CWE reconstruction	✗	✓	✗	✗	✓	✓	✓
Real GB curtailment data	Partial	✓	✗	✗	✗	✗	✓
Long-term planning	✗	✗	Partial	✗	✗	Partial	✓
Electrolyser performance detail	Partial	Partial	✗	✓	✗	Partial	✓
Hydrogen storage sizing	Partial	Partial	✗	Partial	✓	Partial	✓
Generalisable planning framework	✗	✗	Partial	✗	✗	✗	✓

Note: ✓ indicates that the modelling feature is included; ✗ indicates that the modelling feature is not included.

2. Techno-Economic Modelling

This section presents a techno-economic modelling framework for hydrogen production from renewable energy, with a focus on utilising curtailed wind energy through electrolysis. The methodology involves data collection and conversion, technical system modelling, performance evaluation, and economic assessment to evaluate the feasibility of hydrogen generation and storage.

A schematic of the HGSS system is shown in Figure 1. The underlying premise is that a wind farm is electrically connected to a co-located hydrogen generation and storage system, where power that would otherwise be curtailed (P_{curt}) is redirected from the grid to supply a PEM electrolyser through a suitable power converter. Curtailment is treated as an exogenous, site-specific input that reflects observed network constraints, rather than as a controllable design variable.

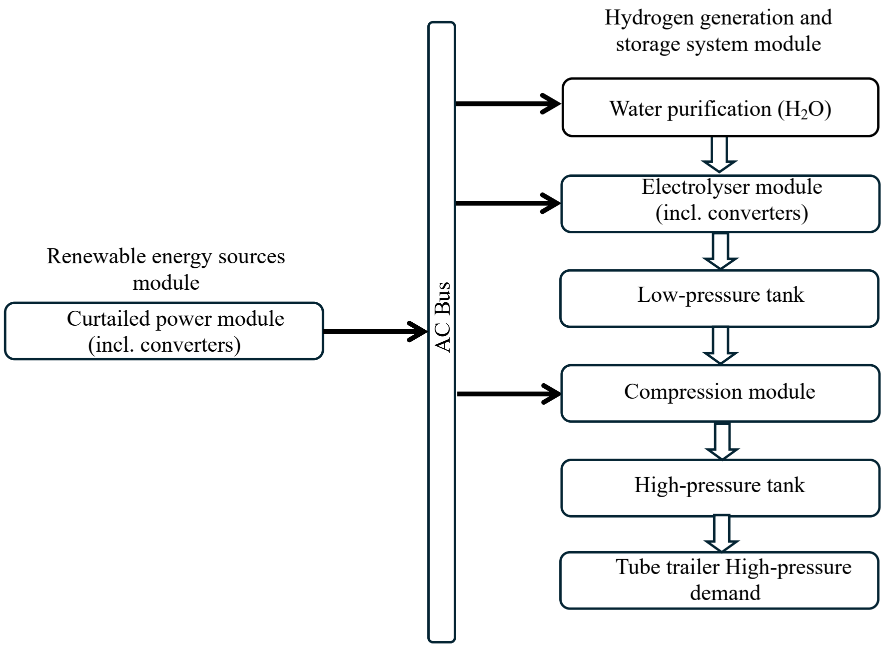

Figure 1. Simplified hydrogen generation and storage system block diagram.

The demand side of the system is shared among the electrolyser, water purification unit, and compressor, which together represent the main electricity-consuming components of the HGSS. The electrolyser output is variable on a mass basis, and the hydrogen mass production rate ($\dot{m}_{H_2}$) is preferred because mass is invariant to pressure and, therefore, conserved through compression/expansion; it also aligns directly with the economic objectives LCOH (£/kg) and revenue (£/kg), and can be readily converted to energy using the lower heating value (LHV). Accordingly, the electrical set-point P_{elr} (kW) is mapped to the hydrogen mass production rate via the stack-specific energy consumption (kg/kWh), which embeds efficiency and degradation effects. A high-level control system, serving as an energy management system, is necessary to operate the system. The model integrates CWE, electrolysis, and hydrogen storage to assess both technical performance and economic viability.

Although individual modules of the studied system have been reported in previous studies, their integration within a unified framework for curtailed-wind-powered hydrogen generation and storage remains limited. Therefore, while certain modelling elements inevitably resemble existing approaches because of the inherent characteristics of the system components, the overall modelling structure and integration presented in this work are original, particularly in their unified formulation and application to system-level assessment.

2.1. Technical Modelling

The HGSS comprises multiple interconnected subsystems, including a CWE interface, power transformation and conversion equipment, electrolysers, and hydrogen compression and storage units. The system is designed using a modular architecture that enables flexible integration of these components and allows the modelling framework to be applied to different curtailment-driven hydrogen production scenarios are discussed in the following sections.

2.1.1. Modelling of Curtailed Wind Energy

Accurate system simulation requires realistic wind input data. In wind energy feasibility studies, power output can be estimated either from theoretical wind-speed equations or directly from the turbine manufacturer's power curve. The theoretical approach requires detailed turbine parameters that are often unavailable and must separately account for operational limits. In contrast, the manufacturer's power curve already reflects real operating constraints and validated performance data. Therefore, the power-curve method is used in this study for reliability and simplicity. Wind speed data are commonly recorded at a standard reference height, typically 10 m above ground level, which differs from the actual hub height of utility-scale wind turbines. Since wind speed increases with altitude due to reduced surface friction, the measured values must be adjusted to the turbine hub height. This is achieved using either the power-law or logarithmic wind-profile law to obtain a more representative hub-height wind speed. See Equation (1).

$$U(z) = U_{z_{\mathrm{ref}}} \times \frac{\ln\left(\frac{z}{z_0}\right)}{\ln\left(\frac{z_{\mathrm{ref}}}{z_0}\right)} \tag{1}$$

In this equation, z and z_{ref} represent the hub and reference heights (m), $U(z)$ and $U_{z_{\mathrm{ref}}}$ denote wind speeds at those respective heights (m/s), and z_0 is the surface roughness length (m). This correction ensures that the wind speeds reflect the turbine rotor's actual operating conditions. The corrected hub-height wind speed is converted into electrical power output using the manufacturer's validated power curve for the reference turbine, as shown in Figure 2. Accordingly, the wind turbine power output, $P_{\mathrm{wt}}(t)$, is calculated from the corrected wind speed using the power curve, as expressed in Equation (2).

$$P_{\mathrm{wt}}(t) = f_{pc} \times (U(z)(t)) \tag{2}$$

where f_{pc} represents a nonlinear mapping of wind speed to turbine power output, constructed from the manufacturer's published power curve data, typically implemented using an interpolation technique.

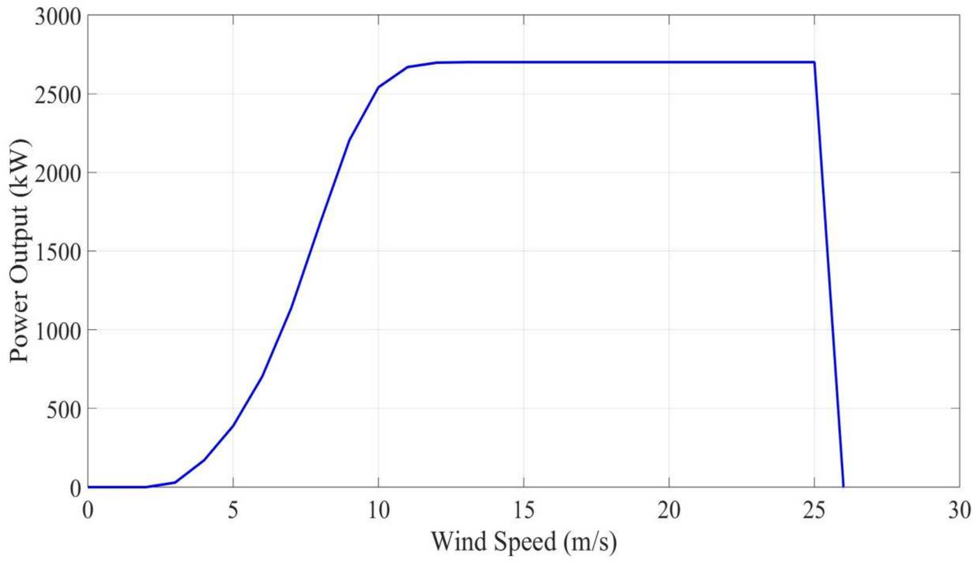

Figure 2. The wind power curve for the wind turbine [22].

The technically available wind turbine power is not assumed to be fully dispatchable, as grid constraints and network congestion lead to measurable wind curtailment. Publicly available datasets report curtailment as aggregated curtailed energy values (MWh) over defined reporting periods [23], as illustrated in Figure 3. However, these datasets do not provide explicit system-operator dispatch signals at hourly or sub-hourly resolution. Since dynamic electrolysis and hydrogen storage modelling require sub-daily temporal resolution to accurately capture power–mass–flow interactions, the aggregated curtailment data cannot be directly implemented within the simulation framework. Instead, the reported curtailed energy values are used as an energy constraint to reconstruct representative hourly curtailed power profiles.

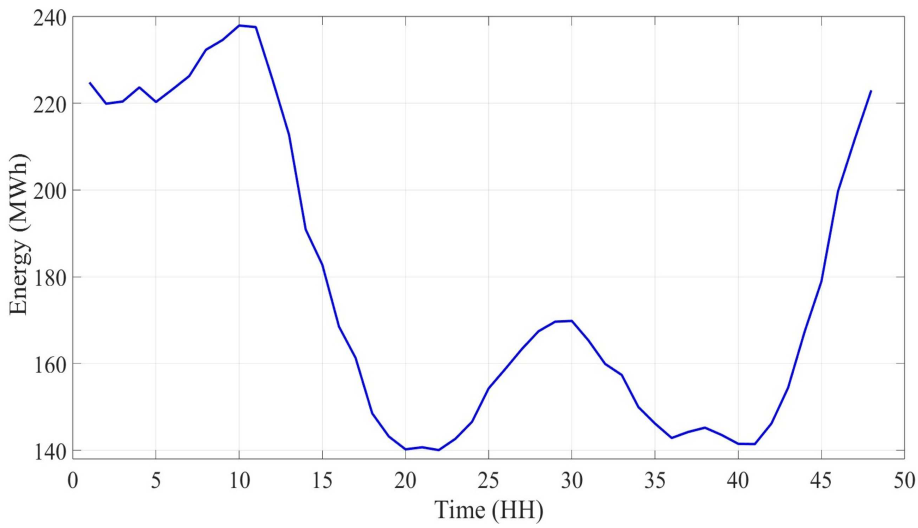

Figure 3. Daily wind energy curtailment [23].

Specifically, monthly-average diurnal curtailment profiles are constructed by averaging three years of observed curtailment data (2021–2023). This yields a representative intra-day curtailed energy distribution for each month, preserving seasonal and daily variability while ensuring compatibility with the time-resolved hydrogen energy storage model. In general, CWE in power system datasets is reported as aggregated energy quantities rather than dispatch-level power signals. To enable dynamic power-balance modelling and integration with time-resolved subsystem models (e.g., electrolysers, compressors, and auxiliary loads), CWE must, therefore, be reconstructed into a time-resolved power profile.

The reconstruction process utilises hourly wind speed data as input to a wind turbine power-curve model to estimate the instantaneous available wind power output $P_{\mathrm{wt}}(t)$. A normalised curtailment factor $P_{\mathrm{curt,norm}}$ is derived from processed curtailment statistics and represents the fraction of available wind power curtailed at each time step. The element-wise multiplication of $P_{\mathrm{wt}}(t)$ and $P_{\mathrm{curt,norm}}$ yields the curtailed wind power $P_{\mathrm{curt}}(t)$, which defines the renewable power available for hydrogen production. Further details regarding the CWE reconstruction workflow and its validation are presented in the following subsection.

The average curtailed energy is calculated in Equation (3):

$$E_{\mathrm{HH,avg}}(t) = \frac{1}{N}\sum_{y=1}^{N} E_y(t) \quad [\mathrm{MWh}] \tag{3}$$

Here, $E_{\mathrm{HH,avg}}(t)$ is the multi-year average half-hourly curtailed energy, while N represents the number of years considered, and $E_y(t)$ is curtailed energy at time interval (t)in year y The hourly curtailed power is then reconstructed from the averaged half-hourly curtailed energy using Equation (4):

$$P_{\mathrm{curt,avg}}(t) = \frac{E_{\mathrm{HH,avg}}(t)}{\Delta t} \quad [\mathrm{MW}] \tag{4}$$

Here, $P_{\mathrm{curt,avg}}(t)$ represents reconstructed hourly curtailed energy consistent with the observed daily totals, rather than directly measured dispatch actions, Δt is duration of that interval (in half hour). In the third step, the curtailed power is normalised by the installed capacity, as given in Equation (5):

$$P_{\mathrm{curt,norm}}(t) = \frac{P_{\mathrm{curt,avg}}(t)}{P_{\mathrm{Inst,Cap}}} \quad [-] \tag{5}$$

The curtailed power profile is then calculated by multiplying the normalised curtailment factor by the wind turbine power output, as shown in Equation (6):

$$P_{\mathrm{curt}}(t) = P_{\mathrm{curt,norm}}(t) \times P_{\mathrm{wt}}(t) \quad [\mathrm{kW}] \tag{6}$$

The resulting hourly curtailment profiles represent a statistically consistent approximation of intra-day curtailment behaviour, rather than an exact replication of grid operator dispatch actions. This approach preserves the magnitude, seasonal distribution, and variability of curtailed energy while enabling dynamic simulation of electrolyser operation, hydrogen compression, and storage. It is appropriate for the planning-oriented objectives of this study, which focus on long-term electrolyser utilisation and techno-economic performance over multi-year horizons.

2.1.2. Electrolyser Model

Electrical Power Conversion to Electrolyser

The modelled curtailed wind power $P_{\mathrm{curt}}(t)$ passes through an electrical conversion stage, including a transformer and AC/DC and DC/DC converters, to model their losses and obtain the net input power of the electrolyser P_{elr} [kW]. Each stage introduces efficiency losses, represented by Equation (7):

$$\eta_{\mathrm{conv,total}} = \eta_{\mathrm{transformer}} \times \eta_{\mathrm{AC-DC}} \times \eta_{\mathrm{DC-DC}} \tag{7}$$

In this study, an overall conversion efficiency of 96% is assumed, implying approximately 4% losses across all stages. The net DC power delivered to the electrolyser, therefore, reflects practical conversion losses rather than idealised turbine output. Accurately modelling these losses is essential, as electrolyser performance and hydrogen production are directly dependent on the effective DC input power. Finally, the electrical power available to the HGSS $P_{\text{hgss}}(t)$, is obtained by applying the overall power conversion efficiency to the available curtailed wind power, as given in Equation (8):

$$P_{\text{hgss}}(t) = \eta_{\text{conv,total}} \times P_{\text{curt}}(t) \tag{8}$$

where $P_{\text{hgss}}(t)$ represents the effective DC power supplied to the HGSS after accounting for transformer and converter losses, and $\eta_{\text{conv,total}}$ denotes the aggregate electrical conversion efficiency. This formulation incorporates practical conversion losses and ensures that the power delivered to the electrolyser reflects realistic system conditions.

Power Constraints and Control Model

The electrolyser is modelled as a power-driven device, where the input electrical power determines the hydrogen production rate. The instantaneous electrolyser input power $P_{\text{elr}}(t)$ is constrained by (i) available curtailed wind power, (ii) conversion losses, (iii) allowable operating power bands, and (iv) ramp-rate limitations. The overall constrained power is expressed as

$$P_{\text{elr}}(t) = f_{\text{rr}}\Big(f_{\text{rl}}\Big(\eta_{\text{conv,total}}\big(P_{\text{hgss}}(t) - P_{\text{comp}}(t) - P_{\text{pump}}(t)\big)\Big)\Big) \tag{9}$$

where $P_{\text{hgss}}(t)$ is the total available curtailed wind power, $P_{\text{comp}}(t)$ is the compressor power demand, $P_{\text{pump}}(t)$ is the water pump power demand, $\eta_{\text{conv,total}}$ represents conversion and electrical losses, f_{rr} is a saturation function enforcing allowable power bands, and f_{rl} is a rate limiter modelling ramp-rate constraints. This formulation ensures that auxiliary loads are first deducted from the available renewable power, that conversion losses are then applied, and that operational constraints are finally enforced.

The electrolyser must operate within a predefined power range to avoid degradation at low current densities and to respect its rated capacity:

$$P_{\text{elr,min}}(t) \leq P_{\text{elr}}(t) \leq P_{\text{elr,nom}}(t) \tag{10}$$

where $P_{\text{elr,min}}$ is the minimum allowable operating power and $P_{\text{elr,nom}}$ is the rated (nominal) power.

Additionally, electrolyser operation is limited by the available curtailed wind power, ensuring that hydrogen production does not exceed renewable energy availability:

$$P_{\text{elr}}(t) \leq P_{\text{curt}}(t) \tag{11}$$

To prevent excessive electrical and mechanical stress, the electrolyser input power must satisfy ramp-rate limits:

$$-R_{\text{p,down}} \leq \frac{P_{\text{elr}}(t) - P_{\text{elr}}(t-\Delta t)}{\Delta t} \leq R_{\text{p,up}} \tag{12}$$

The electrolyser ramp-rate limits during start-up and shutdown are calculated as

$$R_{\text{p,up}} = \frac{P_{\text{elr,nom}}}{T_{\text{startup}}} \tag{13}$$

$$R_{\text{p,down}} = \frac{P_{\text{elr,nom}}}{T_{\text{shutdown}}} \tag{14}$$

with $R_{\text{p,up}}$ and $R_{\text{p,down}}$ defined as positive magnitudes [W/s]. T_{startup} and T_{shutdown} denote the required times to ramp between zero and rated power.
Since the electrolyser is power-driven, the hydrogen production rate is derived from the constrained input power:

$$\dot{m}_{\text{H}_2}(t) = \eta_{\text{stack}}(t) \cdot P_{\text{elr}}(t) \tag{15}$$

where η_{stack} is the electrolyser efficiency in [kg/kWh]. This formulation ensures dimensional consistency and reflects that hydrogen output is determined by electrical input power.

A supervisory logic controller determines the electrolyser demand $P_{\text{elr,d}}$ based on the state-of-charge of the low-pressure hydrogen tank (LPT) SOC_{lpt}. This enables real-time adjustment of hydrogen production, allowing the electrolyser to operate dynamically between on and off states, as shown in Figure 4. The control logic is implemented using logical operators and an S–R flip-flop block to determine the electrolyser operating status based on storage levels. Specifically, the electrolyser is switched on when the SOC_{lpt} falls below a certain threshold of its capacity and remains active until the SOC_{lpt} reaches its defined upper limit $SOC_{\text{lpt,max}}$. Conversely, when the LPT approaches full capacity, the shutdown signal is triggered to prevent overfilling.

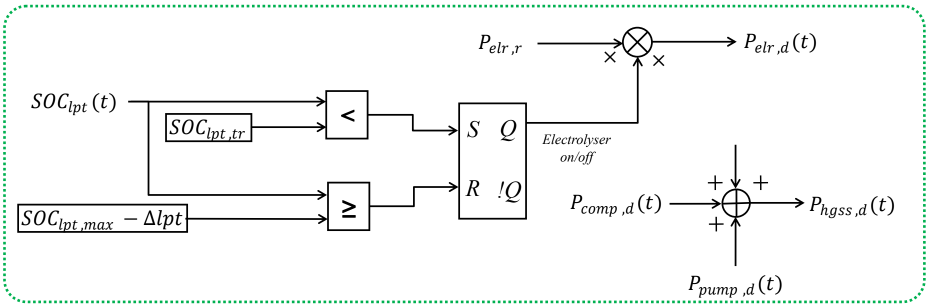

Figure 4. Electrolyser logic control and demand model. The logic ensures that the electrolyser operates only when the hydrogen SOC_{lpt} is below a specified threshold and shuts down when the main tank reaches its upper limit.

Energy Use and Degradation Over Lifetime Model

To determine the total lifetime energy consumption of the electrolyser stack, manufacturer-provided performance data are used, including the stack efficiency, η_{stack}, as shown in Figure 5, and the expected stack degradation rate. These parameters are used to estimate the cumulative energy consumption of the stack over its lifetime and to inform the scheduling of stack replacements. Because the model is driven by curtailed hourly wind data, intra-hour power variability must be approximated when estimating stack energy consumption. For this purpose, preliminary simulations assume that the stack operates at low power for part of the hour and at rated power for the remainder. This assumption is not used for dispatch or operational control of the electrolyser; rather, it is introduced solely to estimate the lifetime energy throughput required for manufacturer-based lookup of stack degradation and end-of-life. This approach corresponds to Equations (16)–(19). Sensitivity to this assumption is not investigated in this study, since stack lifetime is assumed to depend primarily on cumulative energy throughput rather than short-term power fluctuations. Figure 6 shows, in the lower section, how the model accumulates lifetime energy consumption and schedules stack replacements based on total energy use. The energy consumed during low-power and rated-power operation is calculated using the following equations:

$$E_{\text{stack,l,p}} = \frac{elr_{\text{lp}} \cdot \dot{m}_{\text{H}_2}}{\eta_{\text{stack}}} \quad [\text{kWh}] \tag{16}$$

$$E_{\text{stack,r,p}} = \frac{elr_{\text{rp}} \cdot \dot{m}_{\text{H}_2}}{\eta_{\text{stack}}} \quad [\text{kWh}] \tag{17}$$

$$E_{\text{stack,total}} = E_{\text{stack,l,p}} + E_{\text{stack,r,p}} \quad [\text{kWh}] \tag{18}$$

The average lifetime energy requirement is obtained as

$$E_{\text{lifetime}} = \frac{E_{\text{stack,total}}}{2} \quad [\text{kWh}] \tag{19}$$

where $E_{\text{stack,lp}}$ and $E_{\text{stack,rp}}$ represent the energy used during low-power and rated-power operation, respectively. In contrast, $E_{\text{stack,total}}$ is the cumulative energy consumption over the stack lifetime. The terms elr_{lp} and elr_{rp} reflect the respective portions of operating time in each mode.

To improve efficiency under variable-power conditions, the minimum operating power threshold can be lowered by partitioning the system into multiple stacks. For example, a single 2 MW stack with a 10% minimum load requires 200 kW, whereas two 1 MW stacks reduce this minimum to 100 kW, increasing operational flexibility under limited renewable availability [24]. Only the electrolyser stack is modelled with explicit replacement over the 20-year project lifetime. All other major system components (balance-of-plant, compression units, and hydrogen storage vessels) are assumed to have technical lifetimes equal to or exceeding the analysis horizon and are, therefore, not replaced [25,26].

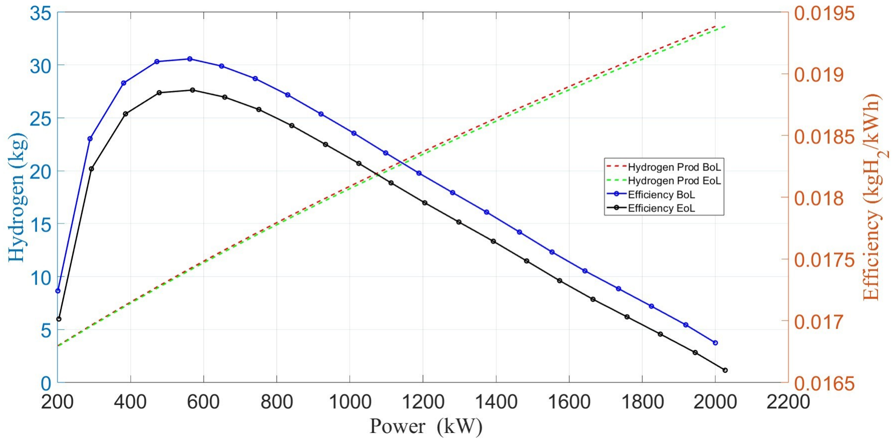

Figure 5. Performance curve of ITM Power PEM electrolyser stack, including its hydrogen production and efficiency when the stack is at BoL and at its EoL [27].

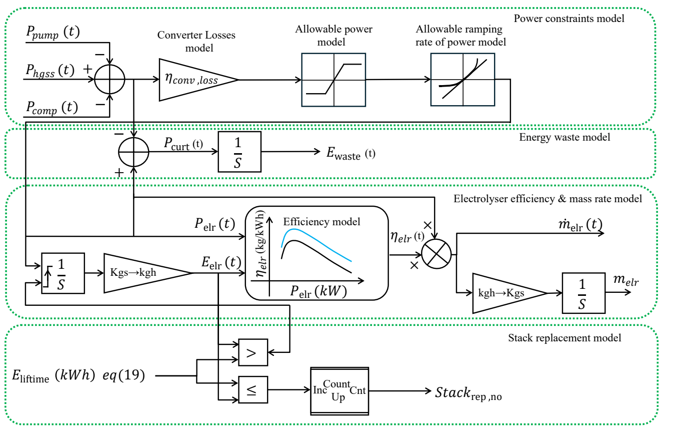

Figure 6. PEM electrolyser model showing the power constraints, energy waste, efficiency, mass flow rate, and stack replacement sub-models.

Stack Efficiency and Hydrogen Production Model

The performance of a PEM electrolyser stack degrades over time, primarily reducing its efficiency. This decline manifests in two ways: either a reduction in hydrogen output at a fixed input power, or an increase in power consumption to maintain constant hydrogen production. In practical systems, the second approach is typically used to ensure a stable hydrogen supply. The stack efficiency, η_{stack}, defines the mass of hydrogen produced per unit of electrical energy consumed. It is calculated as

$$\eta_{\text{stack}} = \frac{3600 \cdot \dot{m}_{\text{H}_2}}{P_{\text{elr}}} \quad [\text{kg H}_2/\text{kWh}] \tag{20}$$

Figure 5 illustrates the relationship between input power and efficiency for a typical PEM electrolyser. As the input power increases, efficiency rises until it peaks at approximately 600 kW, after which it declines. This behaviour is modelled using a two-dimensional lookup table that links electrical input to hydrogen output. The model also incorporates stack degradation as a function of cumulative energy throughput [27]. Commercial PEM electrolysers typically operate at efficiencies ranging from 56.3% to 69.4%. Table 3 provides an overview of efficiency data from various manufacturers. The system configuration used in this study is shown in Figure 6, which presents the detailed PEM electrolyser model implemented for simulation.

Table 3. Overview of efficiency for commercial PEM electrolysers.

PEM Supplier	Nominal Power (MW)	Pressure (bar)	E-Cons. (kWh/Nm^3)	η_{LHV} (%)	Overall Efficiency	Ref.
ITM Power	0.7	20–80	5.5	54	System	[28]
ITM Power	1	20	5.02–6.24	56.3–69.4	System	[27]
Giner Inc.	2	40	5	60	n.a.	[29]
Hydrogenics	1.5	30	5–5.4	56–60	System	[30]
Siemens	1.25	35	5.1–5.4	56–69	System	[31]
AREVA H_2Gen	0.13	35	4.4	68	System	[32]
Proton OnSite	0.25	30	5	60	System	[33]
HYLYZER	1	30	3.6–4.3	40–48	Stack	[10]
H-TEC	0.06	30/50	4.5	67	System	[34]
Angstrom Advanced	0.06	4	5.8	52	n.a.	[35]
KOBELCO Eco-Sol	0.06	4–8	5.5–6.5	46–55	n.a.	[36]
GreenHydrogen	0.01	50	5.5	55	Stack	[37]
Sylatech	0.01	30	4.9	61	System	[38]
IEA	–	–	–	63–68	System	[39]

2.1.3. Water Purification Module

Water consumption for hydrogen production is modelled using a practical value rather than the stoichiometric minimum. Electrolysis requires approximately 9 L of ultrapure water per kilogram of hydrogen based on stoichiometric conversion. In practice, additional makeup water is required to account for water losses through drainage, purification, membrane hydration, and evaporation, as well as auxiliary circulation within the plant. Industrial data reported by ITM Power indicate that total water usage in PEM electrolysers can reach approximately 27 L H_2O/ kg H_2, of which roughly one third passes through purification processes and enters the plant [27]. In this study, a representative specific water consumption of 27 L/kg H_2 is adopted for hydrogen production, capturing the dominant makeup water requirements while maintaining a planning-oriented modelling scope consistent with techno-economic assessments [19].

Since the water purification module model is simplified to its electrical pump power representation, it is integrated directly within the electrolyser module. Figure 6 illustrates the electrolyser hardware modelling framework, including the associated water supply system. Because hydrogen production varies with the available electrical input power, the required water flow rate adjusts dynamically to match the instantaneous hydrogen generation rate. When the electrolyser is offline, water consumption is assumed to be zero. The volumetric water demand, q_{H_2O}, is, therefore, expressed as

$$q_{H_2O} = \dot{m}_{H_2} \times k_{H_2O} \quad [\text{L/h}] \tag{21}$$

where $\dot{m}_{H_2}$ denotes the hydrogen production rate (kg/h), and k_{H_2O} represents the specific water requirement per kilogram of hydrogen produced. Since variations in water flow directly influence the auxiliary electrical demand, the pump power consumption, P_{pump}, is calculated as

$$P_{\text{pump}} = \frac{\gamma \times q_{H_2O} \times H}{\eta_{\text{pump}}} \quad [\text{kW}] \tag{22}$$

where γ is the specific weight of water (N/m^3), H is the hydraulic head (m), and η_{pump} is the mechanical efficiency of the pump. This formulation ensures that water is supplied only during hydrogen production, while the associated auxiliary energy demand is consistently accounted for in the integrated electrolyser model.

2.2. Storage Low/High Pressure Tank and Control Modules

Hydrogen storage within the proposed system is organised as a three-layer configuration comprising a 20 bar low-pressure buffer tank, a 350-bar high-pressure tank, and a 200-bar tube trailer. Each component serves a distinct operational function and adheres to a consistent modelling framework based on mass balance and thermodynamic relationships.

Hydrogen produced by the electrolyser first enters the low-pressure buffer tank (20 bar). The buffer tank acts as a dynamic decoupling element, smoothing short-term production fluctuations and protecting downstream components, particularly the compressor and electrolyser, from rapid pressure variations [27]. When activated, the compressor incrementally pressurises hydrogen from 20 bar to 350 bar, after which the gas is directed either to the high-pressure tank (main storage) or to a connected tube trailer through a direct-fill process. The main storage system comprises a set of cylinders, each rated at 50 kg, enabling large-scale hydrogen accumulation for delivery. During periods without active hydrogen production (i.e., compressor idle state), hydrogen can be transferred from the main tank to a tube trailer via pressure equalisation, governed by the gas law, until the trailer pressure approaches approximately 200 bar.

For system-level mass tracking and SOC estimation, hydrogen storage is modelled using the ideal gas law:

$$P_{\text{tk}} V_{\text{tk}} = nRT \tag{23}$$

where P_{tk} is the internal pressure, V_{tk} is the tank volume, n is the number of moles of hydrogen, R is the universal gas constant, and T is the gas temperature. The stored hydrogen mass is, therefore, obtained as

$$\dot{m}_{H_2}(t) = \frac{P_{\text{tk}}(t) V_{\text{tk}} M_{h_2}}{RT_{\text{tk}}} \tag{24}$$

where M_{h_2} is the molar mass of hydrogen.

The tank input hydrogen management sub-module regulates the mass inflow to the storage tank to prevent overfilling and maintain safe operating conditions. As illustrated in Figure 7, the sub-module receives a commanded hydrogen inflow rate $\dot{m}_{tk,in}$, representing the requested mass transfer into the tank.

At each sampling instant, the available remaining storage capacity, $M_{\text{tk,rem}}(t)$, based on the SOC margin, is calculated using Equation (27). Based on this remaining capacity, the maximum allowable inflow rate, $\dot{m}_{\text{tk,in,max}}(t)$, is determined from Equation (28). The actual inflow rate delivered to the tank, $\dot{m}_{\text{tk,in}}(t)$, is then determined by comparing the requested inflow with both the SOC constraint and the allowable inflow limit. Full acceptance of the requested inflow is only permitted when the tank state of charge satisfies

$$SOC_{\text{tk}}(t) < SOC_{\text{tk,max}} \tag{25}$$

and when the requested inflow does not exceed the allowable limit,

$$\dot{m}_{\text{tk,in,d}}(t) \leq \dot{m}_{\text{tk,in,max}}(t) \tag{26}$$

The available remaining storage capacity is expressed as

$$M_{\text{tk,rem}}(t) = \frac{\left|SOC_{\text{tk,max}} - SOC_{\text{tk}}(t)\right|}{100} \cdot Tank_{\text{nom,cap}} \quad [\text{kg}] \tag{27}$$

where $Tank_{\text{nom,cap}}$ is the nominal hydrogen storage capacity of the tank in kg.

Accordingly, the maximum allowable tank inflow rate is given by

$$\dot{m}_{\text{tk,in,max}}(t) = \frac{M_{\text{tk,rem}}(t)}{Sample_{\text{rate}}} \quad [\text{kg/s}] \tag{28}$$

where $Sample_{\text{rate}}$ is the control sampling interval. If either condition in Equations (25) and (26) is violated, the input management block limits or suppresses the inflow accordingly, as illustrated in Figure 7. This prevents overfilling of the tank and avoids excessive compressor backpressure.

Similarly, the tank output hydrogen management sub-module governs hydrogen withdrawal from the storage tank. As illustrated in Figure 7, the lower logic control receives a requested output mass flow rate, $\dot{m}_{\text{tk,out,d}}(t)$, corresponding to hydrogen delivery requirements, such as trailer filling or downstream consumption. At each time step, the available stored hydrogen mass, $M_{\text{tk,av}}(t)$, is evaluated using Equation (31). Based on this available mass, the maximum allowable discharge rate, $\dot{m}_{\text{tk,out,max}}(t)$, is obtained from Equation (32). The actual tank output mass flow rate, $\dot{m}_{\text{tk,out}}(t)$, is then determined by enforcing both the minimum SOC constraint and the discharge flow limit. Full withdrawal of the requested demand is only allowed when

$$SOC_{\text{tk}}(t) > SOC_{\text{tk,min}} \tag{29}$$

and

$$\dot{m}_{\text{tk,out,d}}(t) \leq \dot{m}_{\text{tk,out,max}}(t). \tag{30}$$

The available hydrogen mass for discharge is expressed as

$$M_{\text{tk,av}}(t) = \frac{\left|SOC_{\text{tk}}(t) - SOC_{\text{tk,min}}\right|}{100} \cdot Tank_{\text{nom,cap}} \quad [\text{kg}] \tag{31}$$

Accordingly, the maximum allowable output mass flow rate is given by

$$\dot{m}_{\text{tk,out,max}}(t) = \frac{M_{\text{tk,av}}(t)}{Sample_{\text{rate}}} \quad [\text{kg/s}] \tag{32}$$

where $SOC_{\text{tk}}(t)$ is the real-time tank state of charge, $SOC_{\text{tk,max}}$ and $SOC_{\text{tk,min}}$ are the maximum and minimum allowable SOC limits, respectively, $Tank_{\text{nom,cap}}$ is the nominal hydrogen storage capacity in kg, and $Sample_{\text{rate}}$ is the control sampling interval. If the tank SOC approaches its lower bound or if the requested outflow exceeds the maximum allowable discharge rate, the control logic proportionally limits the output flow. Alternative operating conditions are summarised in the decision logic presented in Figure 7, the bottom logic control. To ensure safe and stable operation, the tank SOC is constrained within predefined limits:

$$SOC_{\text{tk,min}} \leq SOC_{\text{tk}}(t) \leq SOC_{\text{tk,max}} \tag{33}$$

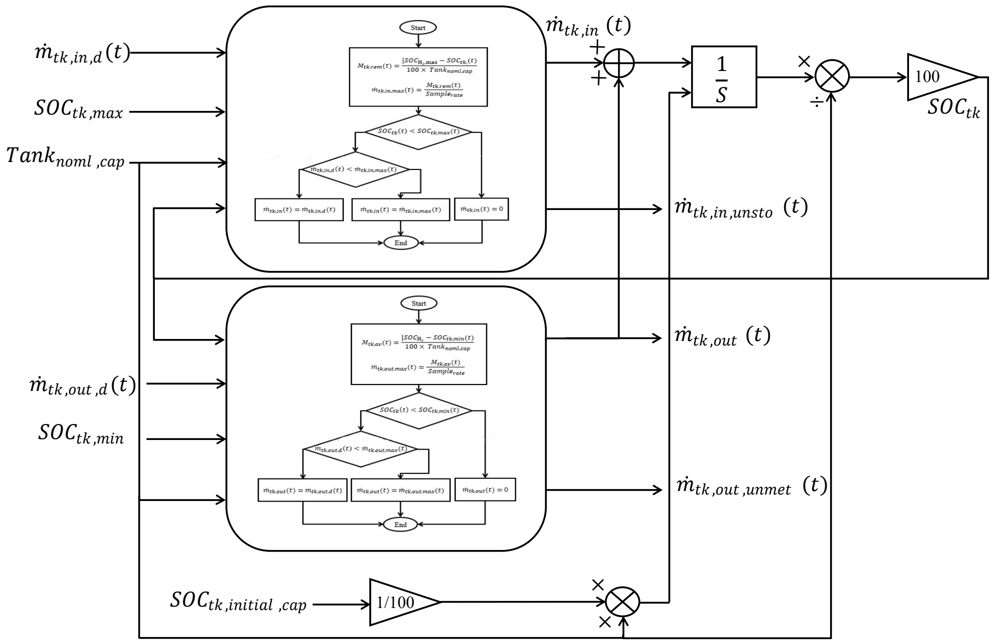

Figure 7. Schematic of the hydrogen tank model illustrating the interconnection between hydrogen input/output management and the tank state of charge (SOC).

The storage tank formulation presented in this section provides a generalised modelling framework that applies to both the low-pressure tank (buffer) and the high-pressure storage tank (main). For clarity and compact notation, the generic symbol *tk* denotes a storage tank in the system throughout this subsection. In the following HGSS interconnection section, the same tank model is applied to each storage component. The subscripts are replaced to represent the low-pressure (lpt) and high-pressure (hpt) tanks.

Hydrogen storage at 350 bar is modelled using the ideal-gas formulation for system-level mass balance and SOC estimation. While hydrogen exhibits non-ideal behaviour at elevated pressures, higher-fidelity real-gas models are primarily required for detailed thermodynamic and mechanical vessel design [1,40]. Published 350 bar storage data suggest that the ideal-gas assumption may overestimate the stored hydrogen mass by approximately 15–20%. Nevertheless, for the planning-oriented techno-economic assessment undertaken in this work, the ideal-gas approximation is considered sufficient, since the analysis is focused on comparative sizing and performance trends rather than exact vessel thermodynamics. This modelling assumption is, therefore, retained and explicitly acknowledged as a limitation of the present study.

2.3. Compression Module

In addition to the PEM electrolyser, the compressor and associated valves (including pressure reduction devices) play a key role in regulating hydrogen transfer between storage levels. The electrolyser produces hydrogen at low pressure (typically 20 bar), which is unsuitable for high-pressure storage due to hydrogen's low volumetric density. Therefore, a fixed-speed compressor is used to raise the pressure to the main storage level (up to 350 bar) [27,41]. In this study, the compressor is modelled with a fixed mass flow rate and rated electrical power (i.e., the compressor demand power is assumed equal to its rated power when operating). The compressor mass flow rate is fixed at 40 kg/h.

The compressor is modelled as a steady-state control volume, with no accumulation within the compression stage. Consequently, the inlet and outlet mass flow rates are equal:

$$\dot{m}_{\mathrm{comp,in}}(t) = \dot{m}_{\mathrm{comp,out}}(t) = \dot{m}_{\mathrm{comp}}(t). \tag{34}$$

Manufacturer data are commonly provided as volumetric flow at normal conditions, $\dot{V}_{\mathrm{N}}$ in $\mathrm{Nm^3/h}$, defined at $(P_{\mathrm{N}}, T_{\mathrm{N}})$. This is converted to suction conditions $(P_{\mathrm{s}}, T_{\mathrm{s}})$ using the ideal gas relationship:

$$\dot{V}_{\mathrm{s}}(t) = \dot{V}_{\mathrm{N}}\left(\frac{P_{\mathrm{N}}}{P_{\mathrm{s}}(t)}\right)\left(\frac{T_{\mathrm{s}}(t)}{T_{\mathrm{N}}}\right), \tag{35}$$

and the discharge-side volumetric flow at $(P_{\mathrm{d}}, T_{\mathrm{d}})$ is

$$\dot{V}_{\mathrm{d}}(t) = \dot{V}_{\mathrm{s}}(t)\left(\frac{P_{\mathrm{s}}(t)}{P_{\mathrm{d}}(t)}\right)\left(\frac{T_{\mathrm{d}}(t)}{T_{\mathrm{s}}(t)}\right). \tag{36}$$

Assuming ideal gas behaviour, the hydrogen mass flow rate can be written at suction or discharge conditions as

$$\dot{m}_{\mathrm{comp}}(t) = \frac{P_{\mathrm{s}}(t)\, M_{\mathrm{h_2}}}{R\, T_{\mathrm{s}}(t)}\, \dot{V}_{\mathrm{s}}(t) = \frac{P_{\mathrm{d}}(t)\, M_{\mathrm{h_2}}}{R\, T_{\mathrm{d}}(t)}\, \dot{V}_{\mathrm{d}}(t), \tag{37}$$

where $M_{\mathrm{h_2}}$ is the molar mass of hydrogen and R is the universal gas constant.

To remain consistent with the fixed-speed compressor assumption, the compressor mass flow is limited to a fixed value when operating:

$$\dot{m}_{\mathrm{comp}}(t) = C_{\mathrm{comp}}(t) \times \dot{m}_{\mathrm{comp,r}} \tag{38}$$

where $C_{\mathrm{comp}}(t) \in \{0, 1\}$ is the compressor operating state (1 = ON, 0 = OFF), as shown in Figure 8. Similarly, the compressor electrical demand is assumed equal to the rated power whenever the compressor is ON:

$$P_{\mathrm{comp}}(t) = C_{\mathrm{comp}}(t)\, P_{\mathrm{comp,r}}. \tag{39}$$

This treatment follows the same modelling philosophy adopted in the reference study, where fixed-speed operation permits the compressor to be represented using manufacturer-rated specifications while preserving computational efficiency for long-horizon simulations. The compressor transfers hydrogen from the LPT to the HPT. Its operation is governed by the tank's state of charge, ensuring that compression occurs only when sufficient hydrogen is available at the suction side and storage headroom exists at the discharge side. The compressor is enabled when the HPT SOC drops below a refill threshold, and the LPT SOC remains above a minimum threshold:

$$C_{\mathrm{comp}}(t) = \begin{cases} 1, & SOC_{\mathrm{hpt}}(t) \leq SOC_{\mathrm{hpt,tr}} \;\wedge\; SOC_{\mathrm{lpt}}(t) > SOC_{\mathrm{lpt,tr2}} \\ 0, & SOC_{\mathrm{hpt}}(t) \geq SOC_{\mathrm{hpt,max}} - \Delta_{\mathrm{hpt}} \;\vee\; SOC_{\mathrm{lpt}}(t) < SOC_{\mathrm{lpt,min}} + \Delta_{\mathrm{lpt}} \end{cases} \tag{40}$$

where $SOC_{\mathrm{hpt,tr}}$ is the HPT refill trigger threshold, $SOC_{\mathrm{lpt,tr2}}$ is the minimum LPT threshold required to allow reliable compressor operation, and Δ_{hpt}, Δ_{lpt} represent small hysteresis margins (e.g., 1%) introduced to avoid rapid switching.

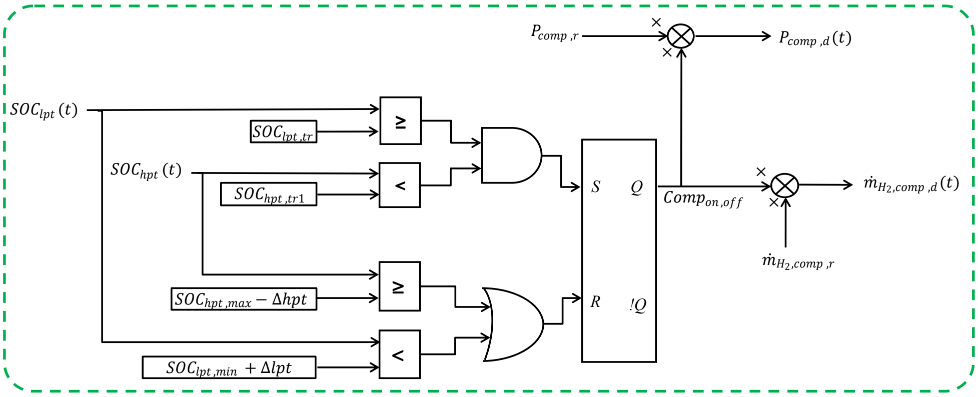

Figure 8. Logic control and demand compressor modelling.

Although this simplification may affect the detailed prediction of compressor power consumption under certain operating conditions, it does not affect the main objective of the present study, which is to perform a system-level planning and sizing assessment.

2.4. Energy Management System Model

The overall operation of the HGSS is coordinated by a supervisory energy management system (EMS), which determines how curtailed renewable power is utilised at the system level. At this stage of the modelling, the EMS does not describe the detailed internal control of individual submodules; rather, it governs the overall power balance between the available curtailed power and the total electrical power required by the HGSS.

The main function of the EMS is to compare the available curtailed renewable power, $P_{\mathrm{curt,av}}(t)$, with the total HGSS power demand, $P_{\mathrm{hgss,d}}(t)$. Based on this comparison, the controller determines the actual power that can be supplied to the system, $P_{\mathrm{hgss}}(t)$, as well as any remaining curtailed power that cannot be utilised and is, therefore, treated as excess or passed power, $P_{\mathrm{Pass}}(t)$. In this way, the EMS acts as the supervisory layer that links renewable energy availability to the operation of the complete hydrogen generation and storage system. The total requested power of the HGSS equals the sum of the electrical demands of its main system components. It is evaluated as

$$P_{\mathrm{hgss}} = P_{\mathrm{elr,r}} + P_{\mathrm{comp,r}} + P_{\mathrm{pump,r}} \tag{41}$$

where $P_{\mathrm{elr,r}}$ is the rated/nominal electrolyser power demand, $P_{\mathrm{comp,r}}$ is the compressor power demand, and $P_{\mathrm{pump,r}}$ is the power consumed by the water pump.

2.5. Hydrogen Generation and Storage System Modules Interconnection

Figures 9 and 10 illustrate the overall integration of the hydrogen generation and storage system and its global energy management structure. Figure 9 presents the interconnections among all main submodules of the HGSS. Each submodule has been developed previously, and the relevant equations, figures, and detailed descriptions are referenced within the corresponding blocks. These interconnected submodules together form the complete HGSS model on the demand side of the studied system.

Figure 10 depicts the system's overall energy management logic. At this level, the total available curtailed renewable energy source (RES) power, $P_{\mathrm{curt}}(t)$, is continuously compared with the total electrical power demand of the HGSS, $P_{\mathrm{hgss,d}}(t)$. Based on this comparison, the model determines the direct curtailed power supplied to the HGSS and the surplus curtailed power that is rejected as spillage. Accordingly, the total electrical power available to the HGSS, $P_{\mathrm{hgss,av}}(t)$, represents the curtailed RES power effectively delivered to the system. From a system integration perspective, the HGSS model links the electrolyser, compressor, low-pressure tank, and high-pressure tank submodules through mass-flow, power-flow, and control-signal interactions. The hydrogen mass flow demand, $\dot{m}_{\mathrm{hgss,d}}(t)$, is the principal input to the HGSS and to the overall studied system, as it defines the required hydrogen production level. In response, the interconnected submodules operate in a coordinated manner to deliver the actual hydrogen production rate, $\dot{m}_{\mathrm{hgss}}(t)$, which is considered the final output of the system and is later used in the calculation of key performance indicators.

For the LPT and HPT submodules, the internal variables are presented in a form consistent with the general tank model shown in Figure 7. However, the subscripts lpt and hpt are used instead of tk to distinguish the variables of the low and high-pressure tanks. From the electrical power modelling viewpoint, the main power-related variables of the integrated HGSS are $P_{\mathrm{hgss,av}}(t)$ and $P_{\mathrm{hgss,d}}(t)$, which describe the available input power and the system demand, respectively. In operational terms, the complete system is governed by coordinated control logic distributed across the major submodules. This includes the electrolyser control unit described in Section Energy Use and Degradation Over Lifetime Model and shown in Figure 4, the compressor control unit presented in Section 2.3 and Figure 8, and the global energy management strategy between the RES and the electrolyser described in Section 2.4 and Figure 10. In addition to these individual controllers, overall coordination among the main modules is embedded in the system's control structure to ensure reliable and consistent operation under varying power availability and hydrogen demand. The corresponding control interactions are introduced within the modelling of each submodule and collectively define the supervisory logic of the complete HGSS.

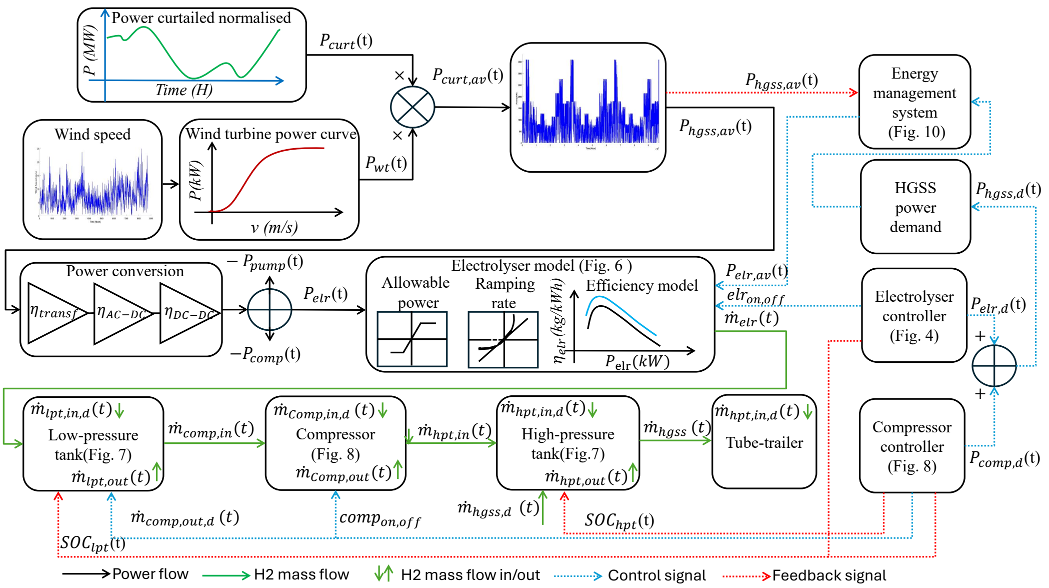

Figure 9. The configuration and interconnection of the principal modules of the studied renewable curtailed power supplying the hydrogen generation and storage system are presented in Figure 1.

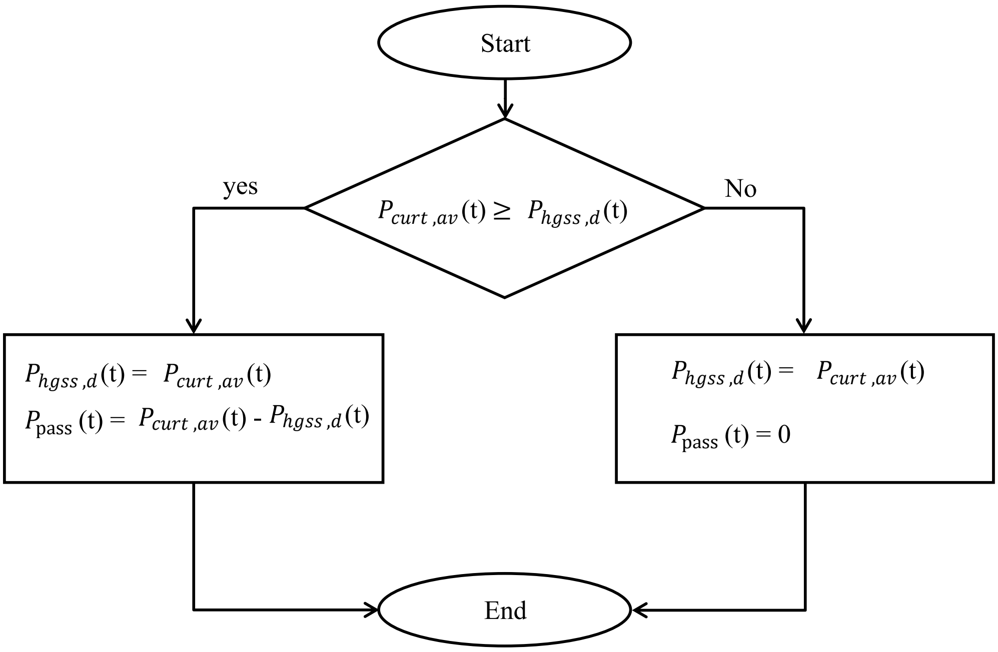

Figure 10. Logic model of the power balance part of the global energy management module.

2.6. Economic Model

In addition to the technical assessment, an economic model is developed to evaluate the cost performance and overall viability of the HGSS under different design configurations. The role of this model is to provide an economic basis for comparing alternative system sizes and operating conditions, while remaining fully linked to the technical outputs obtained from the simulation results. Accordingly, the economic analysis is used to determine whether a technically feasible configuration can also deliver favourable economic performance.

The economic assessment considers the principal indicators adopted in this study, including CAPEX, OPEX, LCOH, NPV, and payback period. These indicators are derived from the simulated operation of the system, such that hydrogen production, power consumption, operating duration, and storage behaviour are directly reflected in the corresponding economic results.

The cost model includes the major investment items required for the HGSS, such as the electrolyser, compressor, hydrogen storage units, and associated balance-of-plant and installation costs, together with the main operating costs, including electricity, water use, maintenance, and component replacement where relevant. Since the proposed system is driven by curtailed wind energy, its economic performance depends strongly on the extent to which curtailed energy can be converted into useful hydrogen. Therefore, the technical and economic analyses are closely integrated throughout this study. The present analysis is intended to support planning and comparative design assessment rather than to represent a detailed commercial financing case. Its purpose is to identify economically favourable sizing trends and to examine how the main design variables influence hydrogen production cost over the project lifetime.

The economic analysis adopts a system-level planning perspective and applies a discount rate to represent the time value of money and the cost of capital. Rather than modelling a detailed debt-equity financing structure, the present study uses a parametric range of discount rates in order to test the sensitivity of the results to financing assumptions. This approach is appropriate for comparative sizing analysis, where the primary objective is to identify robust design trends rather than to replicate the financing structure of a specific commercial project.

2.6.1. Economic Performance Indicators

The economic performance of the HGSS is evaluated using the main indicators: CAPEX, OPEX, LCOH, and NPV. Together, these metrics provide a consistent basis for assessing the investment requirement, hydrogen production cost, and overall financial viability of the proposed system over the project lifetime.

CAPEX represents the initial investment required to establish the HGSS. This study covers the major plant components for hydrogen production, including the electrolyser, compressor, hydrogen storage units, and associated balance-of-plant and installation costs. The total CAPEX of the HGSS can, therefore, be expressed as

$$CAPEX_{\mathrm{hgss}} = \sum_{k=1}^{N_{\mathrm{hgss}}} CAPEX_y \tag{42}$$

where N_{hgss} is the number of costed HGSS components and $CAPEX_y$ is the capital cost of the yth component. To evaluate the long-term cost of hydrogen production, the levelised cost of hydrogen is calculated using a discounted cash flow model. This accounts for the initial capital cost, annual operating costs, electricity purchases, and stack replacement costs over the project lifetime, while also considering the discounted hydrogen production. The LCOH is defined as

$$\mathrm{LCOH} = \frac{CAPEX_{\mathrm{hgss}} + \sum_{t=1}^{T} \frac{C_{\mathrm{stack,rep}}(t) + E_{\mathrm{total,pur}}(t) + OPEX_{\mathrm{hgss}}(t)}{(1+r)^t}}{\sum_{t=1}^{T} \frac{M_{\mathrm{H_2}}(t)}{(1+r)^t}} \tag{43}$$

where $C_{\mathrm{stack,rep}}(t)$ is the stack replacement cost in year t, $E_{\mathrm{total,pur}}(t)$ is the annual electricity expenditure, $OPEX_{\mathrm{hgss}}(t)$ is the annual operating and maintenance cost, $M_{\mathrm{H_2}}(t)$ is the hydrogen produced in year t, r is the discount rate, and T is the project lifetime in years.

In this way, the LCOH reflects both the cost of establishing the system and the effect of long-term operation on the average cost of hydrogen production. Since annual hydrogen output may vary with operating conditions and stack degradation, the discounted hydrogen production is used in the denominator to represent the effective lifetime hydrogen yield of the system. To assess the overall project viability, the present values of expenditures and revenues are also calculated. The present value of total expenditures is given by

$$PV_{\mathrm{Exp}} = \sum_{t=0}^{T} \frac{Exp_t}{(1+r)^t} \tag{44}$$

where Exp_t is the total expenditure in year t, including the initial investment and subsequent annual costs. Similarly, the present value of revenues is

$$PV_{\mathrm{Rev}} = \sum_{t=0}^{T} \frac{Rev_t}{(1+r)^t} \tag{45}$$

where Rev_t is the revenue generated in year t, primarily from hydrogen sales. The net present value is then calculated as the difference between the discounted revenues and discounted expenditures:

$$NPV = PV_{\mathrm{Rev}} - PV_{\mathrm{Exp}} = \sum_{t=0}^{T} \frac{N_t}{(1+r)^t} \tag{46}$$

where N_t is the net cash flow in year t. A positive NPV indicates that the project generates a net economic benefit over its lifetime, whereas a negative NPV implies that the total discounted costs exceed the discounted revenues.

2.6.2. Energy Cost Model

The energy cost model estimates the electricity expenditure associated with operating the HGSS, including the electrolyser and auxiliary components. Electricity prices are derived from historical UK wholesale market data and applied on an hourly basis. Grid electricity prices correspond to UK day-ahead wholesale prices reported by Elexon for the period 2022-2024, expressed in £/MWh [42]. Hydrogen production is curtailed when electricity prices exceed the economic threshold for operation. CWE is assumed to be available at low marginal cost, reflecting its otherwise uncompensated nature under curtailment conditions; however, although curtailed wind energy may in some cases have a very low or even negative effective price, a £0/MWh baseline case is not considered in the present study. Sensitivity to non-zero curtailed energy pricing is examined separately [42]. Transmission and distribution charges are excluded, consistent with a co-located or behind-the-meter operational assumption, and are treated as a modelling simplification for planning purposes.

Electricity expenditure is calculated hourly and aggregated annually as

$$E_{\text{pur},y} = \sum_{t=1}^{8760} \Big(P_{\text{hgss}}(t) \times E_{\text{pur}}(t) \Big) \tag{47}$$

where $P_{\text{hgss}}(t)$ is the HGSS power demand in MW and $E_{\text{pur}}(t)$ is the unit electricity price in £/MWh. The discounted present value of lifetime electricity expenditure is, then,

$$E_{\text{total,pur}} = \sum_{y=1}^{20} \frac{E_{\text{pur},y}}{(1+r)^y} \tag{48}$$

where r is the discount rate (assumed $r = 5\%$).

2.6.3. Electrolyser Cost Model

The electrolyser cost model includes purchase cost C_{elr}, installation/civil works C_{ins}, inverter cost C_{inv}, and stack replacement cost $C_{\text{stack,rep}}$:

$$C_{\text{elr}} = P_{\text{elr,noml}} \times Pur_{\text{kW,elr}} \tag{49}$$

$$C_{\text{ins}} = P_{\text{elr,noml}} \times C_{\text{kW,ins}} \tag{50}$$

$$C_{\text{inv}} = \left(\frac{P_{\text{hgss}}}{P_{\text{rated,inv}}} + 1 \right) \times Pur_{\text{kW,inv}} \tag{51}$$

$$C_{\text{stack,rep}} = P_{\text{elr,noml}} \times Pur_{\text{kW,rep}} \times \text{stack}_{\text{rep,no}} \tag{52}$$

where $Pur_{\text{kW,elr}}$, $C_{\text{kW,ins}}$, $Pur_{\text{kW,inv}}$, and $Pur_{\text{kW,rep}}$ are unit costs, and $\text{stack}_{\text{rep,no}}$ is the expected number of stack replacements over the system lifetime. Balance-of-plant costs are implicitly accounted for in the unit-cost assumptions applied to a fully integrated electrolyser system. Annual electrolyser fixed O&M is estimated at 2.85% of the initial electrolyser cost (excluding stack replacement), consistent with values used in planning-oriented techno-economic studies.

The total electrolyser-related $CAPEX_{elr}$ is

$$C_{\text{elr,total}} = C_{\text{elr}} + C_{\text{inv}} + C_{\text{ins}} \tag{53}$$

2.6.4. Water Cost Model

The model includes the cost of water consumed for hydrogen production. Water demand is computed from the hydrogen production rate using Equation (21), as described in Section 2.1.3. Water costs are evaluated using a constant unit tariff based on UK industrial water prices.

For reproducibility, a representative industrial water price of £3.0/m^3, consistent with values reported in techno-economic hydrogen studies, is assumed [19]. This tariff is applied uniformly over the project lifetime, with no price escalation. Given the relatively small contribution of water costs to total hydrogen production costs, this assumption is considered appropriate for a planning-oriented assessment. Using the adopted specific water consumption, this results in an effective water cost of approximately £0.03 per kilogram of hydrogen produced. The discounted lifetime water demand and cost are then calculated as

$$Q_{\mathrm{H_2O,total}} = \sum_{y=1}^{20} q_{\mathrm{H_2O}}(y) \tag{54}$$

$$C_{\mathrm{H_2O,total}} = Q_{\mathrm{H_2O,total}} \times C_{\mathrm{kg,H_2O}} \tag{55}$$

where $C_{\mathrm{kg,H_2O}}$ is the unit cost of water expressed consistently with the above tariff assumptions. The system is assumed to have access to an existing water connection; therefore, additional infrastructure costs are not included.

2.6.5. Gas Handling Equipment Cost Model

The major gas-handling components include the low-pressure tank, compressor, and high-pressure tank. The storage-system cost and compressor cost are

$$C_{\mathrm{tk}} = tk_{\mathrm{nom,cap}} \times Pur_{\mathrm{kg,tk}} \tag{56}$$

$$C_{\mathrm{comp}} = P_{\mathrm{comp,noml}} \times Pur_{\mathrm{kW,cpr}} \tag{57}$$

where $tk_{\mathrm{noml,cap}}$ is the storage capacity in kg, $P_{\mathrm{comp,noml}}$ is the compressor rated power in kW, and $Pur_{\mathrm{kg,tk}}$ and $Pur_{\mathrm{kW,cpr}}$ are the unit costs. For multiple storage units,

$$C_{\mathrm{tk,total}} = \sum C_{\mathrm{tk}} + C_{\mathrm{comp}}. \tag{58}$$

2.6.6. Total Costs

The total cost of the HGSS is calculated by summing the capital and operational costs of all major components over the system's lifetime. This includes the full cost of the electrolyser, hydrogen storage, and associated equipment. This aggregated cost forms the basis for evaluating the system's economic feasibility using present value methods. It supports key financial metrics such as payback period, LCOH, and NPV, all of which are essential for assessing long-term viability. The total cost is expressed as

$$C_{\mathrm{hgss,total}} = C_{\mathrm{elr,total}} + C_{\mathrm{tk,total}} + C_{\mathrm{H_2O,total}} \tag{59}$$

where $C_{\mathrm{elr,total}}$ represents the total cost of the electrolyser system (including installation, inverters, and replacements), and $C_{\mathrm{tk,total}}$ accounts for the combined cost of storage units and compressor equipment. To improve transparency and directly address cost sensitivity, discounted lifetime expenditure is decomposed into major categories:

$$PV_{\mathrm{Exp}} = PV_{\mathrm{tk}} + PV_{\mathrm{Elec}} + PV_{\mathrm{OM}} + PV_{\mathrm{Water}}, \tag{60}$$

where PV_{tk} includes electrolyser and gas-handling CAPEX and discounted stack replacements; PV_{Elec} is discounted electricity expenditure; PV_{OM} is discounted fixed O&M; and PV_{Water} is discounted water cost.

2.7. Sensitivity Analysis

A sensitivity analysis (SA) approach is applied to identify the optimal sizing of key components in the integrated HGSS system. The focus is on balancing techno-economic performance by varying the configuration of CWE input, electrolyser capacity, and hydrogen storage infrastructure.

Alongside the growing role of hydrogen in the UK's decarbonisation strategy, there is an increasing need for transparent and transferable modelling tools that allow policymakers, infrastructure planners, and industrial stakeholders to understand the renewable generation and storage requirements of large-scale hydrogen systems. In particular, stakeholders require visibility on how a system built around a 2.3 MW PEM electrolyser behaves under realistic operating constraints, and how such a system can be operated to maximise hydrogen production while respecting technical limits. The validation framework adopts a representative hydrogen production system centred around a 2.3 MW PEM electrolyser. The electrolyser is assumed to be an ITM Power unit, and its technical specifications are taken from manufacturer documentation (see Table 4). The stack lifetime is assumed to be 9 years and 7 months, consistent with the reference datasheet. The efficiency curve used in the model is also derived from the manufacturer's performance data and is illustrated in Figure 5.

Table 4. Technical details of the studied system model.

Specifications	**Value (Unit)**	**Specifications**	**Value (Unit)**
Hydrogen generation and storage system module			
Electrolyser		Inlet/suction pressure	20 (bar)
Rated power	2300 (kW)	Inlet H_2 temperature	288 (K)
Water pump rated power	12 (kW)	Outlet/discharge pressure	350 (bar)
Stack EoL	9.7 (y)	**Wind power generation module**	
Cold start-up time	300 (s)	Rated power	2700 (kW)
Shut-down time	2 (s)	Hub height	85 (m)
Max. H_2 production (BoL)	807 (kg/day)	Generator/converter eff.	96/96 (%)
Max. H_2 production (EoL)	691 (kg/day)	**Low/High pressure tank**	
Output hydrogen pressure	20 (bar)	Minimum allowed SOC	5 (%)
Compressor		Maximum allowed SOC	100 (%)
Rated power	100 (kW)	Nominal pressure	20 / 350 (bar)
Volumetric flow rate	450 (Nm^3/h)	Rated capacity	70 / 150 (kg)

To ensure consistency between hydrogen production and downstream system components, a constant hydrogen demand of 33.6 kg/h is imposed. This value corresponds to the maximum continuous hydrogen production rate of a 2.3 MW electrolyser at BoL and reflects realistic operational expectations for industrial operation. The demand is, therefore, not intended to represent a specific end-user, but rather to provide a stable benchmark for validating the dynamic response of the system. The expense terms and unit costs used in the CAPEX and OPEX calculations are summarised in Table 5.

Table 5. Terms of expenses and cost per unit used in CAPEX and OPEX calculations.

Term of Expenses	Cost (Unit)	Term of Expenses	Cost (Unit)
Hydrogen generation and storage system module			
Electrolyser (CAPEX)	1030 (£/kW)	HGSS (OPEX)	(2.5% of CAPEX)/y
Stack replacement	670 (£/kW)	BOP (CAPEX)	1%of HGSS CAPEX
Compressor (CAPEX)	150,000 (£)	Electrical equipment cost (CAPEX)	100,000 (£)
LPT (CAPEX)	750 (£/kg)	HPT (CAPEX)	1200 (£/kg)
Energy cost (OPEX)	35–50 (£/MWh)		

The core subsystems required to represent the hydrogen plant are illustrated in Figure 1 and include the electrolyser and water pump, the hydrogen compressor, the LPT and HPT, and the supervisory control logic. From a system design perspective, compatibility between mass flow rates and pressure levels is enforced across all components. Accordingly, a 100 kW compressor and a 12 kW water pump are selected, consistent with the requirements of a 2.3 MW electrolyser and supported by published technical references.

3. Simulation Results and Discussions

This section presents the simulation results and discussions evaluating the technical performance and economic feasibility of the proposed hydrogen generation and storage system under various planning scenarios. The studied system, which integrates CWE with a hydrogen storage system, is constructed upon the detailed technical and economic framework described in Sections 2.1 and 2.6.

Before analysing system performance and economic outcomes, a multi-level validation is conducted to ensure the physical plausibility of both the reconstructed curtailed wind energy inputs and the dynamic response of the hydrogen generation and storage system. Validation is performed using independent manufacturer specifications, peer-reviewed literature, and publicly available high-level system records, where applicable. This step confirms that the proposed model provides a robust and credible basis for planning-oriented techno-economic assessment.

To quantify the agreement between the reference curtailed wind profile and the reconstructed model output, the mean absolute error (MAE) and mean absolute percentage error (MAPE) were used. MAE measures the average absolute deviation between the two profiles, while MAPE expresses this deviation relative to the reference values in percentage form. These indicators are widely used in model validation studies [43,44]. Their formulations are given in Equations (61) and (62):

$$MAE = \frac{1}{a}\sum_{i=1}^{a}|y_i - x_i| \tag{61}$$

$$MAPE = \frac{100}{a}\sum_{i=1}^{a}\left|\frac{y_i - x_i}{y_i}\right| \tag{62}$$

where a is the number of compared points, y_i is the reference value, and x_i is the reconstructed value. Table 6 illustrates both metrics that were evaluated for the monthly average daily curtailed wind profiles.

Table 6. Validation results for the reconstructed monthly average daily curtailed wind profiles using MAE and MAPE.

Metric	Jan	Feb	Mar	Apr	May	Jun	Jul	Aug	Sep	Oct	Nov	Dec
MAE	0.038	0.055	0.088	0.071	0.066	0.084	0.074	0.037	0.046	0.091	0.073	0.058
MAPE (%)	10.5	8.6	23.3	18.9	26.9	24	22.4	23.9	19.5	21.2	13.2	16.9

In this study, MAE and MAPE were evaluated using the monthly average daily curtailed wind profiles. MAE is expressed in the same unit as the curtailed wind profile, while MAPE is expressed as a percentage. Since MAPE becomes undefined when the reference curtailed wind value is zero, zero-valued reference points were excluded from the MAPE calculation. Therefore, MAE provides a direct measure of the average deviation in curtailed wind magnitude, whereas MAPE provides a relative measure of the deviation between the reconstructed and reference profiles. Figure 11 presents the comparison between reconstructed $P_{\text{curt}}(t)$ Equation (6) and the reference dataset [23], shown as average daily profiles for each month. The reconstructed profiles reproduce the expected seasonal behaviour of curtailed wind energy, with significantly higher curtailed energy during winter months and lower levels during spring and summer. For example, January and February show relatively high curtailed energy levels reaching approximately 4402.3 MWh and 9117.7 MWh, reflecting periods of strong wind generation combined with transmission constraints and system balancing requirements. During these periods, the reconstructed curtailed energy closely follows the reference trend, although the model consistently produces slightly lower values.

In contrast, the spring and summer months, particularly May through September, have approximately 2096.8 MWh of curtailed energy, compared with 2380.0 MWh, indicating a noticeable reduction in curtailed energy. This behaviour is consistent with expected system operation, in which reduced wind availability and increased solar generation influence overall dispatch patterns and congestion levels. The reduced curtailment during these months affects the available energy for hydrogen production and highlights the importance of seasonal variability in evaluating system performance. It is also evident that curtailment does not follow wind speed directly but is influenced by a combination of generation availability, network congestion, and market conditions.

It is important to note that the reconstructed curtailed energy is consistently lower than the reference system-level data across all months. This is an intentional outcome of the reconstruction approach. Due to the absence of high-resolution, site-specific curtailment data, a conservative correction methodology was adopted. Monthly correction factors were applied using historical curtailment data from multiple years, ensuring that the reconstructed curtailed energy does not exceed reported system-level values. This conservative assumption provides a worst-case estimate of available curtailed energy, preventing overestimation of hydrogen production potential in the techno-economic assessment.

Some deviations between reconstructed and reference profiles are more noticeable during the spring and summer months. This is expected, as curtailment behaviour during these periods is influenced by additional system-level factors, including solar generation, electricity demand patterns, and grid congestion conditions. These effects vary throughout the day and across seasons and cannot be fully captured using wind-speed-derived modelling alone. Nevertheless, the reconstructed profiles preserve the overall shape, seasonal variation, and magnitude consistency observed in real curtailment data.

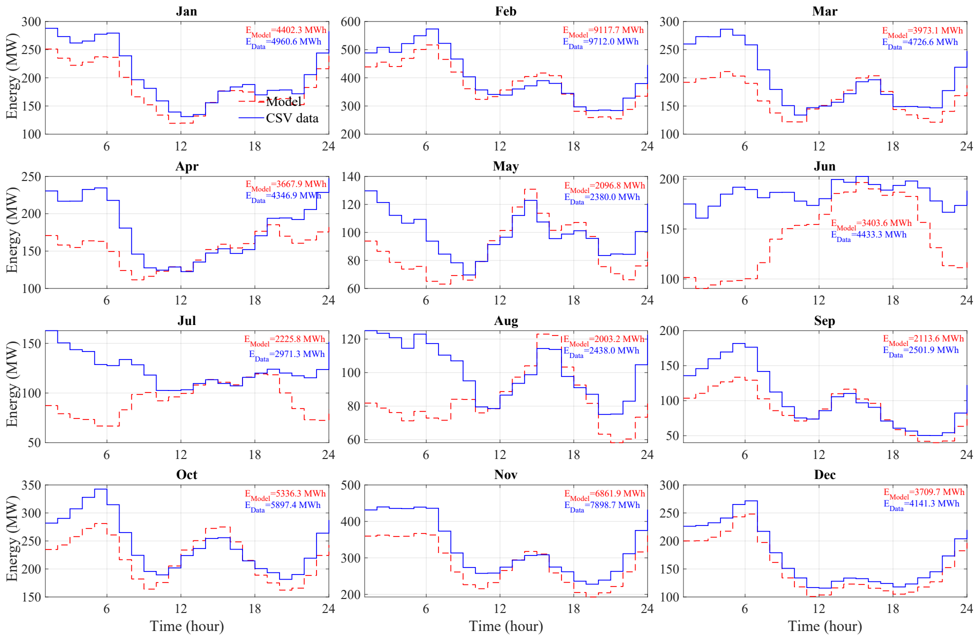

Figure 11. Qualitative validation of reconstructed curtailed wind power profiles against reported system-level curtailment for representative days in selected months of 2022, demonstrating consistent temporal behaviour and seasonal variability.

Overall, the validation confirms that the reconstructed curtailed wind power $P_{\text{curt}}(t)$ profiles provide a realistic and conservative representation of available curtailed energy. Although site-specific validation data were not available, the agreement with system-level behaviour, combined with the conservative modelling assumptions, provides confidence that the reconstructed profiles are suitable for use in the techno-economic analysis of the integrated hydrogen production system.

The electrolyser and associated power conversion stages are validated against manufacturer specifications and literature data, including rated and minimum operating power, ramp-rate limits, conversion efficiency, and specific energy consumption. The model reproduces the expected efficiency trends and operational constraints across the simulated power range, confirming realistic electrochemical and electrical behaviour under variable curtailed power input. Validation of the compression and storage subsystems focuses on hydrogen mass-flow continuity and state-of-charge dynamics across the main storage. Figure 12 shows that the results confirm the physically consistent dynamic behaviour of the electrolyser and storage, and the degradation-related operational assumptions.

Following this validation, the simulation results are presented to evaluate the technical performance and economic feasibility of the proposed hydrogen generation and storage system under a range of planning scenarios. All simulations were conducted in MATLAB 2024a using both the editor and Simulink environments. A cascading, iterative algorithm was employed to adjust key design and operational parameters and observe system responses.

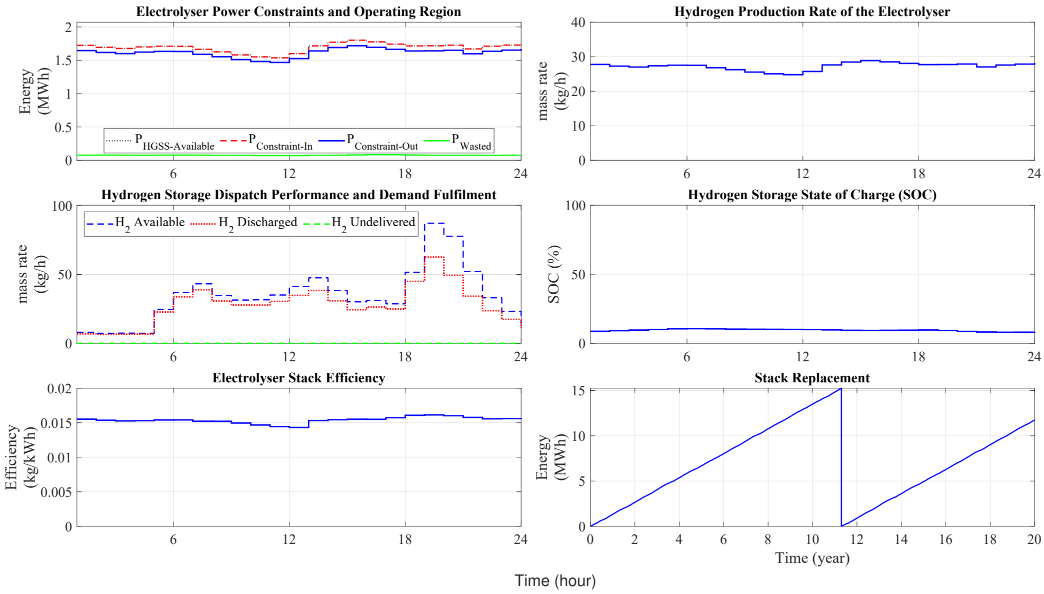

Figure 12. Component-level validation of the proposed hydrogen generation and storage system. The figure demonstrates electrolyser power constraints and operating region under variable curtailed input, hydrogen production rate, hydrogen storage dispatch performance and demand fulfilment, storage state of charge, electrolyser stack efficiency, and stack replacement cycle over the project lifetime.

3.1. Interaction Between CWE and Storage Capacity in Meeting Hydrogen Demand

Figure 13 illustrates the fraction of hydrogen demand met under different combinations of CWE availability and HPT capacity. As expected, increasing CWE improves the system's ability to satisfy hydrogen demand. However, this improvement is non-linear. The most pronounced increase occurs between approximately 50 and 70 MWh of available curtailed energy, beyond which the curves begin to flatten and additional CWE yields only marginal gains in demand fulfilment. This saturation behaviour indicates that, above a certain energy input threshold, system performance becomes increasingly constrained by downstream conversion and storage limitations rather than by energy availability itself. From a system design perspective, this implies that further wind capacity expansion beyond this range would increase electricity availability without proportionate improvements in hydrogen service reliability, thereby reducing overall techno-economic efficiency.

The influence of HPT capacity becomes more noticeable only under higher CWE conditions. Larger storage volumes 164–258 m^3 consistently achieve approximately 97–98.5% demand fulfilment, while smaller tanks 94–141 m^3 remain closer to 96-98% even at elevated CWE levels. Although the absolute difference in performance across tank sizes remains modest (typically within 1–1.5 percentage points), the larger storage capacities provide greater operational robustness, particularly under periods of temporal mismatch between hydrogen production and demand. This suggests that storage sizing primarily contributes to system reliability rather than to total annual hydrogen yield. Importantly, the results demonstrate that hydrogen demand satisfaction is more sensitive to available curtailed energy than to storage capacity over the investigated range. This explains why all storage configurations exhibit nearly parallel performance trends as CWE increases. Only when CWE approaches higher levels (above 60 MWh) does storage capacity begin to act as a limiting factor, as insufficient storage leads to partial loss of producible hydrogen during high-generation periods.

From a system-integration perspective, these findings underscore the importance of coordinating the sizing of energy inputs and hydrogen infrastructure. Oversizing storage without sufficient curtailed energy yields diminishing operational benefits, while oversupplying curtailed energy without adequate storage leads to underutilisation of renewable resources. Therefore, an optimal design region emerges in which CWE availability and storage volume are matched in proportion to maximise both system efficiency and hydrogen supply reliability.

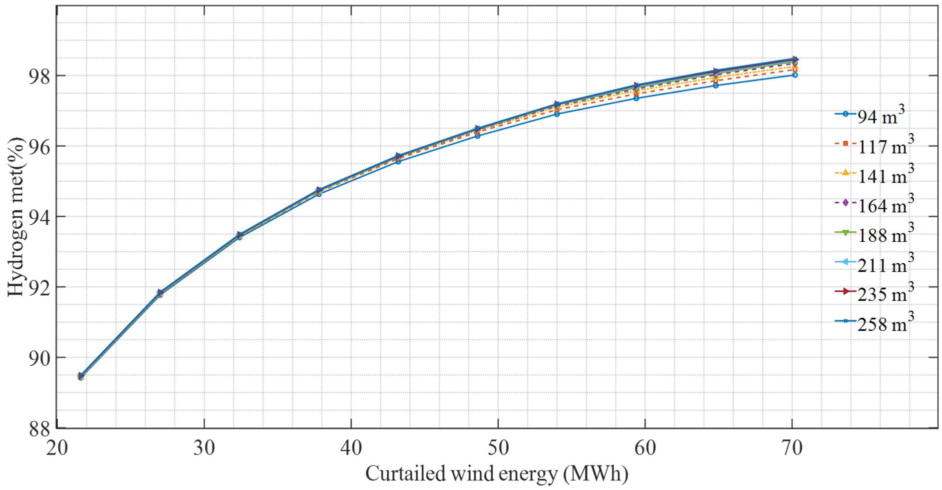

Figure 13. Sensitivity of hydrogen demand fulfilment (%) to available curtailed wind energy (MWh) under different HPT hydrogen capacities (m^3). Results correspond to a 2.3 MW PEM electrolyser with a fixed 75 m^3 LPT; legend values indicate main tank volumes evaluated over the 20-year simulation horizon.

3.2. Impact of Curtailed Wind Energy, Storage Capacity and Financing Assumptions on the Levelised Cost of Hydrogen

Figures 14 and 15 present a sensitivity analysis of the LCOH as a function of available CWE, HPT capacity, and discount rate, while keeping the electrolyser size (2.3 MW) and LPT volume (75 m^3) fixed. Both figures, therefore, evaluate the same underlying system behaviour under different techno-economic assumptions and together provide a consistent assessment of the cost drivers in curtailed-energy-based hydrogen production.

Figure 14 shows that increasing the availability of curtailed wind energy consistently reduces the LCOH across all storage configurations. However, the rate of cost reduction diminishes beyond approximately 60–70 MWh of available CWE, after which additional energy availability yields progressively smaller reductions in the LCOH. This behaviour reflects the curtailment-limited operational nature of the system; at low CWE levels, additional energy significantly improves electrolyser utilisation and spreads fixed capital costs over a larger hydrogen output, whereas at higher CWE levels, utilisation becomes increasingly constrained by storage, compression, and downstream handling limitations.

Increasing HPT capacity also reduces the LCOH, although its effect is less pronounced than that of CWE availability. Larger storage volumes enable greater capture of intermittently produced hydrogen and reduce curtailment-induced losses, particularly under low- to moderate-CWE conditions. At higher CWE levels, however, the marginal benefit of additional storage decreases, indicating that storage oversizing beyond a certain threshold yields diminishing economic returns. These results highlight that optimal system design requires coordinated scaling of both renewable inputs and storage infrastructure, rather than maximising either component in isolation.

Figure 15 complements this analysis by demonstrating the sensitivity of the LCOH to financing assumptions. In the present model, higher discount rates result in systematically lower LCOH values across all CWE levels. This behaviour arises because the discounting framework discounts long-term operating expenditures more strongly than upfront capital investment, thereby lowering the overall levelised cost. Importantly, the relative shape of the curves remains consistent across discount rates, confirming that the underlying technical behaviour of the system is unchanged; rather, the absolute cost level varies with financing assumptions. For example, at high CWE availability, the LCOH decreases from approximately 4.45 £/kg at a 3% discount rate to around 3.15 £/kg at 9%, consistent with the trend of diminishing cost reductions with increasing CWE.

Taken together, Figures 14 and 15 indicate that physical utilisation limits and financial conditions simultaneously constrain curtailed-energy-based hydrogen systems. Under low CWE availability, technical constraints dominate, and improvements in energy input or storage sizing yield significant economic benefits. With higher CWE availability, the system transitions to a capital-dominated regime, in which further cost reductions are primarily constrained by infrastructure utilisation and capital recovery rather than by energy availability. This dual sensitivity highlights the importance of evaluating both techno-operational and financial parameters when assessing the viability of curtailed renewable hydrogen pathways.

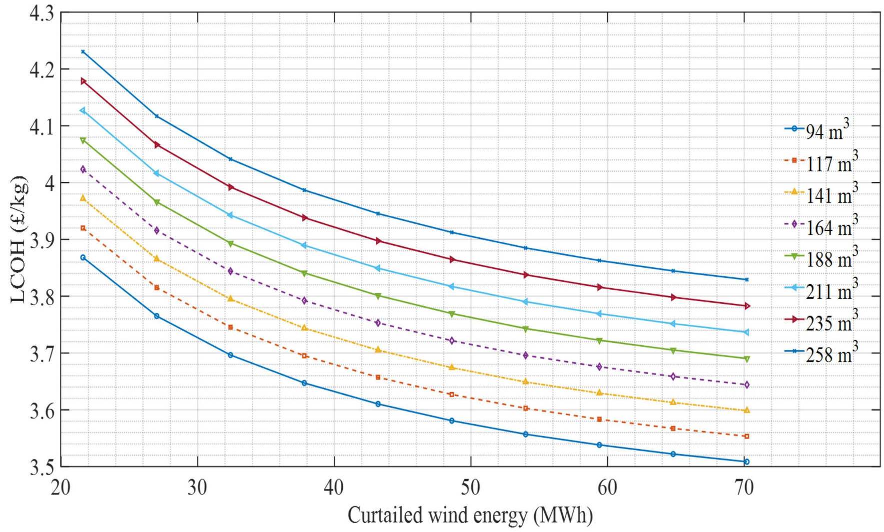

Figure 14. Sensitivity of the LCOH £/kg to available CWE (MWh) under different HPT hydrogen capacities (m^3). Results correspond to a 2.3 MW PEM electrolyser with a fixed 75 m^3 LPT over a 20-year simulation horizon.

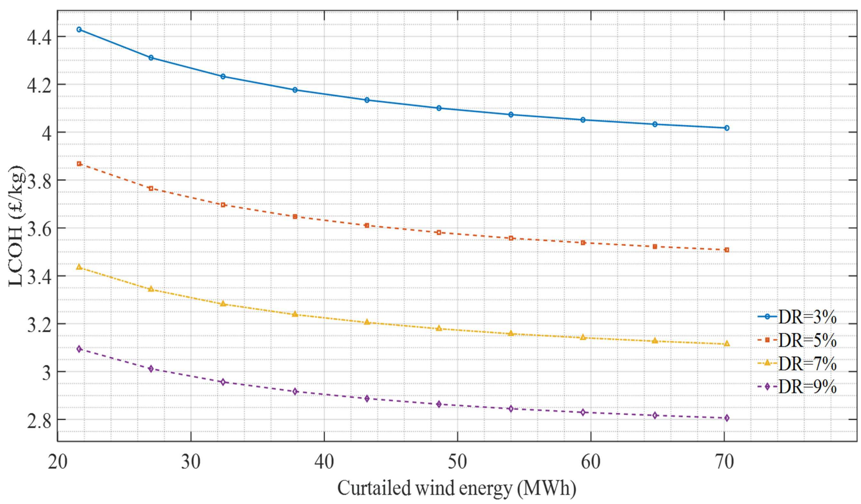

Figure 15. Sensitivity of the LCOH £/kg to available CWE (MWh) under different discount rates. Results correspond to a 2.3 MW PEM electrolyser with a fixed 75 (m^3) LPT over a 20-year simulation horizon.

Figure 16 illustrates the combined influence of CWE availability and main hydrogen storage capacity on the LCOH. Three representative curtailment levels are examined (40, 60, and 70 MWh) to explore system behaviour under low, medium, and high renewable energy availability. For a given storage capacity, higher CWE consistently leads to a lower LCOH. For example, at a main storage volume of approximately 94 m^3, the LCOH is around 3.65 £/kg under 40 MWh availability, compared with approximately 3.52 £/kg and 3.51 £/kg for 60 MWh and 70 MWh, respectively. This confirms that hydrogen production cost in this system is primarily driven by renewable energy availability, since higher CWE improves electrolyser utilisation and distributes capital costs over a larger hydrogen output.

Conversely, for a fixed CWE level, increasing the main storage capacity gradually increases the LCOH. Across all three cases, the LCOH rises modestly as storage increases from around 94 m^3 to 258 m^3. This behaviour reflects the additional capital cost associated with larger storage infrastructure, which is not fully compensated by proportional gains in hydrogen utilisation under the investigated operating conditions. In other words, beyond a moderate storage size, further expansion primarily increases investment cost without delivering equivalent operational benefits.

Importantly, the three curves remain approximately parallel across the storage range, indicating that storage capacity affects the absolute cost level but does not change the underlying sensitivity of the LCOH to energy availability. These results reinforce the conclusions of the previous sections: Curtailed energy availability is the dominant driver of hydrogen costs, and storage infrastructure must be carefully sized to avoid overinvestment.

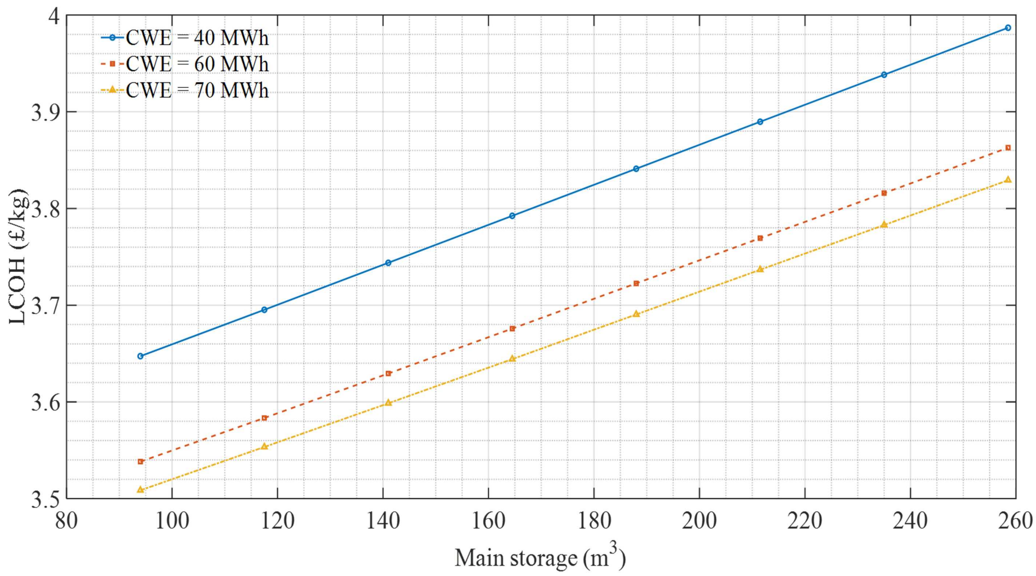

Figure 16. Sensitivity of the LCOH, £/kg to the main storage tank (m^3) under low-mid-high of CWE (MWh). Results are shown for an electrolyser rated at 2.3 MW with a fixed LPT of 75 (m^3) and legend values denote HPT capacities over 20 years.

Figure 17 presents the sensitivity of OPEX to CWE availability for different main hydrogen storage capacities. In contrast to capital expenditure, OPEX is dominated by the discounted cost of electricity for electrolysis and compression, calculated on an hourly basis using representative UK curtailment-linked electricity prices [42]. As expected, OPEX increases with CWE at low-to-moderate curtailment levels (approximately 20–55 MWh), because higher CWE availability increases electrolyser operating hours and, therefore, total electricity consumption.

Beyond approximately 55–60 MWh, the OPEX curves progressively flatten and in some cases exhibit a slight reduction. This non-linear behaviour arises because additional

CWE at high curtailment levels is increasingly supplied during periods associated with very low (and occasionally negative) marginal curtailment prices, thereby reducing the effective average electricity cost (in £/MWh) of the operating profile. Consequently, although hydrogen production continues to increase, the total discounted electricity expenditure does not scale proportionally with CWE, leading to saturation in lifetime OPEX. The similarity in curve shapes across storage configurations indicates that the dominant driver is the electricity price-mix effect rather than storage size.

Larger storage capacities exhibit slightly higher absolute OPEX due to additional compression and auxiliary electricity demand; however, OPEX sensitivity to CWE remains similar across tank sizes. When considered alongside the LCOH trends in Figure 14, this explains why intermediate storage capacities minimise hydrogen costs: They improve operational utilisation and reduce curtailment losses without imposing disproportionate capital recovery costs. Further storage expansion yields diminishing economic returns, as marginal OPEX benefits at high CWE are insufficient to offset the added capital burden.

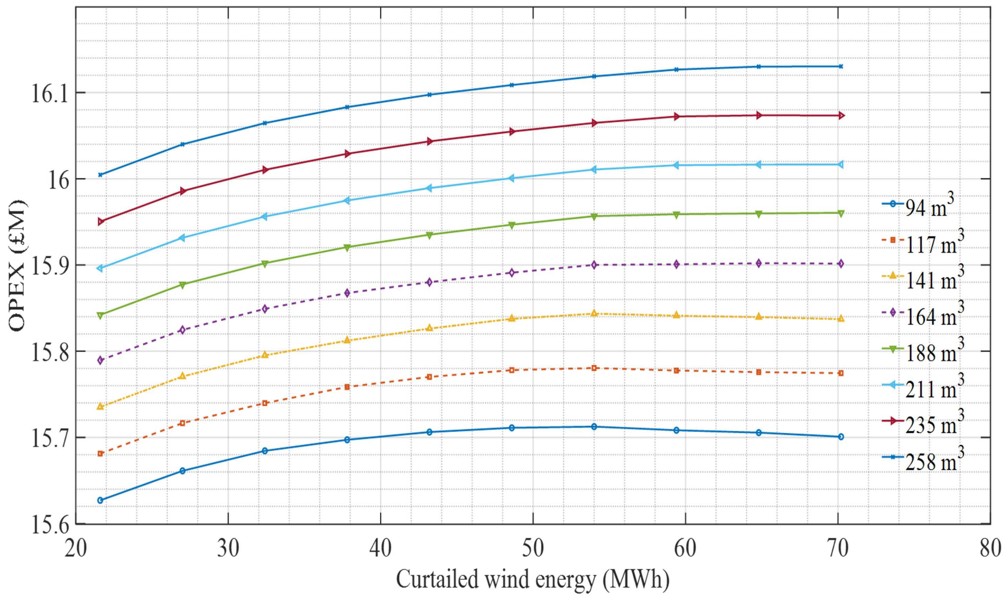

Figure 17. Operating expenditure (OPEX, £ M) as a function of available CWE, (MWh for different HPT capacities (m^3). Results correspond to a 2.3 MW electrolyser with a fixed 75 m^3 LPT over the 20-year horizon.

3.3. Optimal Balance Between CWE and Storage Sizing for Maximising Economic Returns

Figures 18–20 quantify the discounted present value of expenditure (PV_{exp}), discounted present value of revenue (PV_{rev}), and net present value (NPV) for the hydrogen production system over the 20-year project horizon. Collectively, these metrics capture the trade-off between higher renewable energy utilisation (which increases hydrogen output and revenues) and the additional capital and operating requirements associated with larger storage capacities.

Figure 18 shows that PV_{exp} increases modestly with CWE across all storage configurations and is systematically higher for larger main tank capacities. This behaviour is expected because greater availability of higher-CWE increases electrolyser operating hours and associated variable costs (electricity, compression, and auxiliaries). At the same time, larger storage volumes require additional capital investment and related operating overheads. The weak curvature and gradual flattening at high CWE indicate that expenditure does not scale proportionally with CWE, consistent with the saturation effects observed in the OPEX trends. See Section 3.2.

In contrast, PV_{rev} Figure 19 increases strongly with CWE, reflecting higher hydrogen production and sales as more curtailed energy becomes available. The revenue curves gradually plateau at higher CWE levels, indicating diminishing marginal gains once conversion and storage constraints limit further increases in delivered hydrogen (50–70 MWh). Storage size yields only marginal revenue gains, as the curves remain closely clustered, implying that, within the investigated range, the dominant driver of revenue is CWE availability rather than storage expansion.

The resulting NPV trends in Figure 20 highlight the net economic outcome of these competing effects. NPV increases with CWE for all storage sizes, but the rate of increase diminishes at higher CWE values as revenue gains begin to saturate while expenditures continue to accumulate. Importantly, storage capacities (e.g., 94–164 m^3) provide a balanced outcome, maintaining relatively strong NPVs without incurring the higher capital burden associated with the largest storage configuration (258 m^3). This behaviour indicates that, under the present model assumptions, increasing storage size does not necessarily translate into proportionally higher economic returns. This is because the additional storage volume cannot be fully utilised once the system becomes constrained by the electrolyser rated capacity, compressor transfer rate, and fixed hydrogen demand. As also reflected in Figure 13, the increase in hydrogen demand satisfaction becomes relatively small at larger tank sizes, while the associated capital cost continues to rise. Consequently, beyond a certain storage capacity, the additional investment is only weakly recovered, which causes the NPV improvement to diminish and, in some cases, remain marginal.

Finally, Figure 21 shows that higher discount rates reduce NPV across all CWE levels, reflecting the lower present value of future revenue streams under higher financing risk. Consequently, although higher CWE availability improves profitability, project attractiveness becomes increasingly sensitive to the assumed cost of capital, reinforcing the need to evaluate curtailed-energy hydrogen pathways under realistic UK financing conditions.

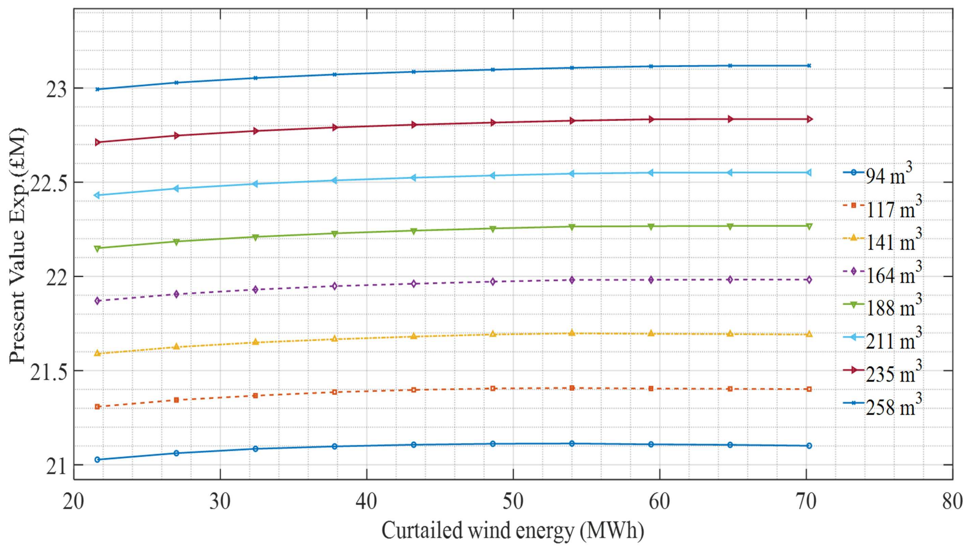

Figure 18. Sensitivity of the present value of expenditure (PV_{exp}, £M) to available WE (MWh) under different HPT capacities (m^3). Results correspond to a 2.3 MW electrolyser with a fixed 75 m^3 LPT over a 20-year horizon. Legend values denote HPT.

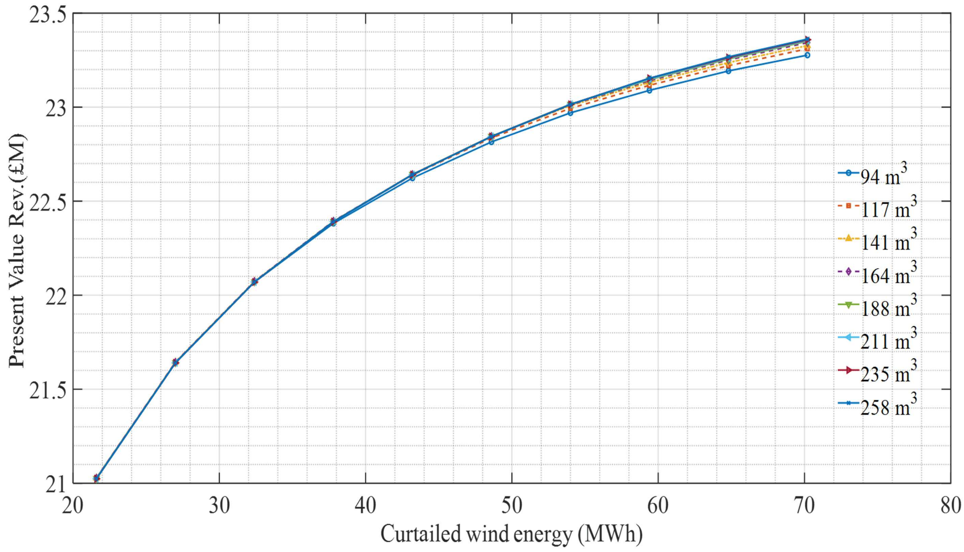

Figure 19. Sensitivity of the present value of revenue (PV_{rev}, £M) to available CWE (MWh) under different HPT capacities (m^3). Results correspond to a 2.3 MW electrolyser with a fixed 75 m^3 LPT over a 20-year horizon. Legend values denote HPT.

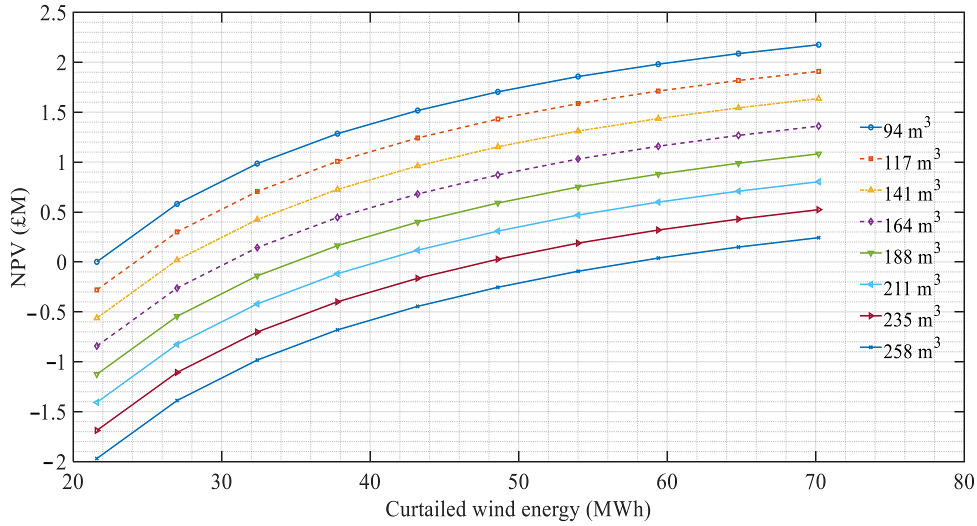

Figure 20. Sensitivity of project net present value (NPV, £M) to available CWE (MWh) under different HPT capacities (m^3). Results correspond to a 2.3 MW electrolyser with a fixed 75 m^3 LPT over a 20-year horizon. Legend values denote HPT.

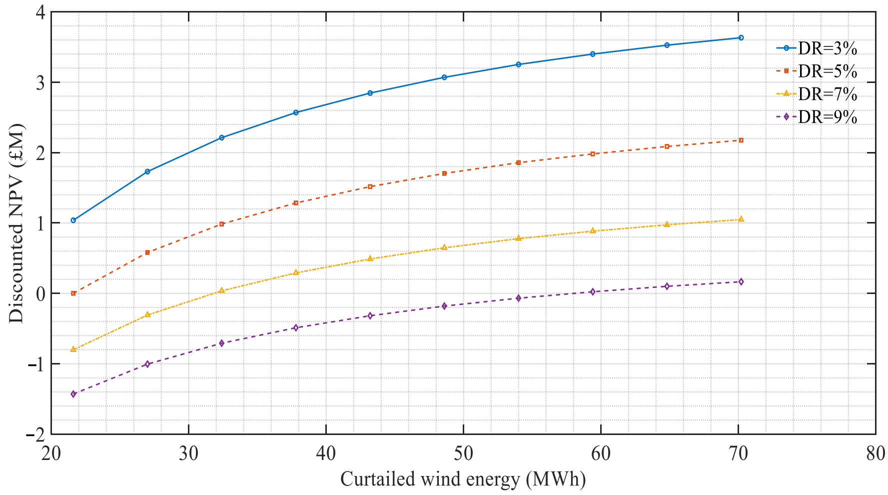

Figure 21. Sensitivity of project net present value (NPV, £M) to available CWE (MWh) under different discount rates. Results correspond to a 2.3 MW electrolyser with a fixed 75 m^3 LPT over a 20-year horizon.

3.4. Comprehensive Sensitivity Analysis of Plant Sizing on Hydrogen Performance and Economics

From a system design perspective, these results highlight the inherently multi-objective nature of planning curtailed energy-based hydrogen systems. While the LCOH remains the most widely used indicator for comparing hydrogen production pathways, relying solely on the LCOH can lead to suboptimal investment decisions. Practical deployment requires simultaneous consideration of additional techno-economic indicators such as NPV, total capital investment, and the proportion of hydrogen demand reliably met.

As shown in Figure 22, the 30 configurations achieving the lowest LCOH were extracted from the full design space and evaluated against additional performance metrics. The first sub-plot indicates that the LCOH varies within a narrow range (approximately 3.5–3.8 £/kg) across these configurations. Although the lowest-LCOH design yields the minimum unit hydrogen cost, it does not necessarily correspond to the most economically attractive system when broader financial performance is considered.

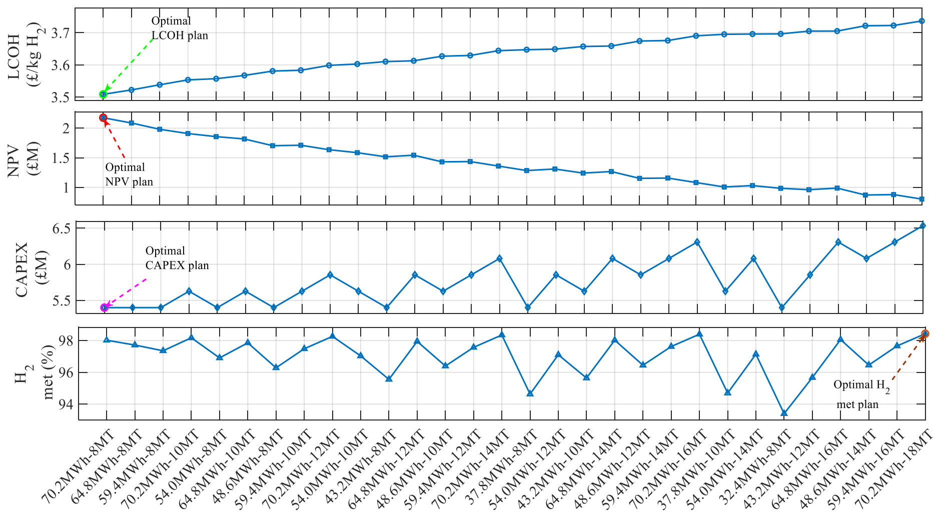

Figure 22. Comparison of the 30 best-performing system configurations ranked by lowest LCOH, showing corresponding values of LCOH (£/kg), NPV (£M), CAPEX (£M), and fraction of hydrogen demand met (%). Each configuration represents a unique combination of curtailed wind energy availability and HPT capacity (MT), with a fixed 2.3 MW electrolyser and 75 m^3 LPT.

The second sub-plot shows the corresponding NPV values. While several low-LCOH configurations exhibit strong profitability, the design with the maximum NPV does not coincide with the absolute minimum LCOH. This highlights a fundamental trade-off between unit cost minimisation and total project value: Configurations with a slightly higher LCOH may achieve higher overall profitability due to increased hydrogen throughput and revenue generation.

The third sub-plot illustrates capital expenditure across the selected configurations. As expected, higher hydrogen production capability and demand coverage are generally associated with increased infrastructure investment, particularly in storage capacity. The fourth subplot shows the fraction of hydrogen demand met, demonstrating that configurations that deliver near-complete demand fulfilment typically require greater investment, thereby reinforcing diminishing economic returns at high levels of system oversizing.

To support practical decision-making, it is, therefore, more informative to identify a subset of "high-performance" designs rather than a single optimal point. Based on the results in Figures 22 and 23, a reduced set of candidate configurations can be selected that satisfy three simultaneous criteria: (i) LCOH close to the global minimum, (ii) positive and competitive NPV, and (iii) high hydrogen demand fulfilment. These shortlisted configurations represent realistic deployment options, enabling system designers or investors to select solutions aligned with their specific priorities (e.g., lowest cost, highest profitability, or highest supply reliability).

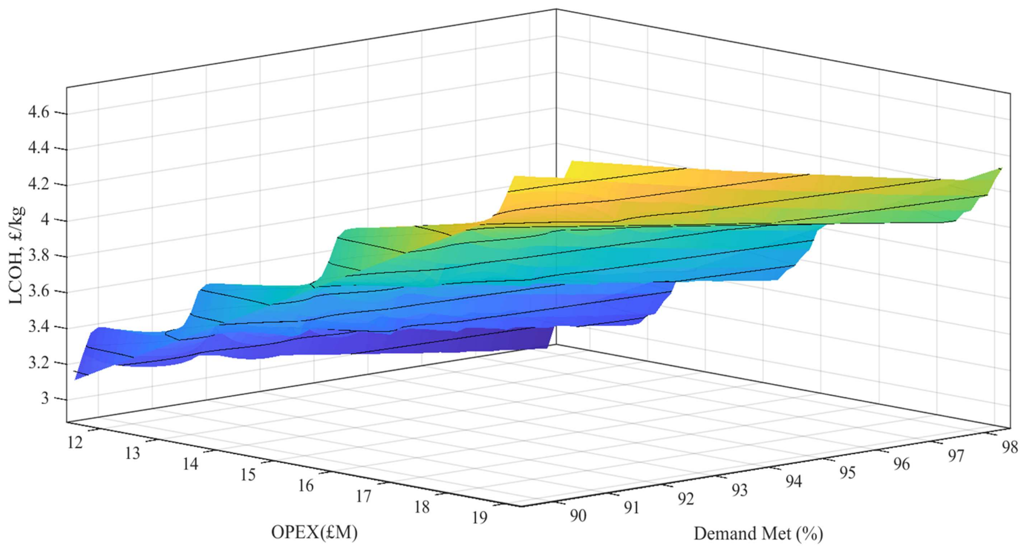

Figure 23. Comprehensive sensitivity surface for all plans, showing how capital expenditure (CAPEX, £M) and the share of hydrogen demand met (%) jointly affect the levelized cost of hydrogen (LCOH, £/kg H_2). The colour scale indicates LCOH magnitude, from lower values in cooler colours to higher values in warmer colours. Configuration 2.3 MW electrolyser; LPT fixed at 75 m^3 over 20 years.

3.5. Optimal System Configuration Based on Levelised Hydrogen Cost and Payback Performance

Figure 24 illustrates the cumulative net present value (NPV, £M) over the 20-year project lifetime. The curve remains negative during the early years because of the high upfront capital investment, then gradually improves as operating revenues accumulate over time. The zero crossing at around year 16 represents the discounted payback point, after which the project begins to generate positive cumulative returns. However, because this occurs relatively late in the project life, only a limited period remains for value creation before the end of the 20-year horizon. This suggests that, under the current assumptions, the project is economically viable but only marginally attractive, with profitability remaining sensitive to key parameters such as the discount rate, hydrogen selling price, and curtailed electricity cost. Overall, the figure indicates that supportive policies or more favourable market conditions could be important for strengthening the investment case.

Accordingly, Table 7 summarises the five most attractive system configurations identified from this multi-objective screening process. These configurations all achieve LCOH values close to 3.51 £/kg, maintain high levels of hydrogen demand coverage (typically above 95%), and deliver favourable NPVs, while avoiding excessive capital oversizing. This structured selection illustrates how the proposed modelling framework can be used not only for cost assessment but also as a practical decision support tool for hydrogen system planning.

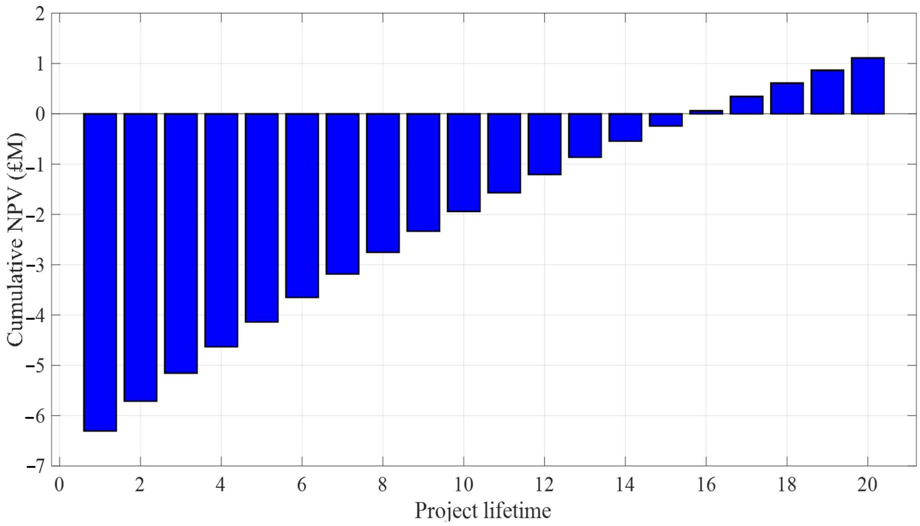

Figure 24. Cumulative net present value (NPV, £ M) over the project lifetime. The zero crossing at year 16 indicates the discounted payback year; subsequent positive values imply value creation at the assumed discount rate.

The optimal LCOH obtained in this study, £3.51/kg H_2, is within the range of values reported in the related literature, although direct comparison should be made cautiously because of differences in system boundaries and assumptions. Ref. [17] reported a base-case LCOH of 5.9 \$/kg H_2(£4.5/kg H_2) for curtailed-renewable hydrogen production, while [19] reported UK wind-tidal hydrogen costs in the mid £3/kg H_2 range depending on configuration. Ref. [18] did not report the LCOH directly but found that wind-based green hydrogen becomes economically viable at prices above about 3 €/kg H_2 (£2.61/kg H_2) under uncertain market conditions. Overall, the differences mainly reflect variations in electricity price assumptions, curtailment treatment, resource conditions, and the selected economic metric.

Table 7. HGSS configurations and associated costs.

System Capacity				CAPEX	LCOH	NPV	MHD
E_{curt} MWh	P_{elr} MW	HPT m^3	LPT m^3	(£M)	(£/kg)	(£M)	(%)
70.2	2.3	94	75	5.4	3.51	2.17	98.01
64.8	2.3	94	75	5.4	3.52	2.08	97.7
59.4	2.3	94	75	5.4	3.259	2.510	97.96
70.2	2.3	117	75	5.6	3.55	1.9	98.1
54.0	2.3	94	75	5.4	3.55	1.8	96.9
64.8	2.3	117	75	5.62	3.56	1.82	97.85

4. Limitations and Future Work

The present study focuses on system-level, planning-oriented techno-economic assessment of a curtailed-wind-driven hydrogen generation and storage system. While the proposed framework provides valuable insights, several limitations are acknowledged and motivate future research directions:

- Ideal-gas modelling at 350 bar simplifies storage behaviour; future work should apply real-gas models for improved thermodynamic accuracy.
- Stack lifetime is based on throughput assumptions; sensitivity to alternative degradation models and operating regimes should be assessed.
- A constant hydrogen demand is assumed in this study as a modelling simplification; future work should incorporate time-varying and seasonal demand profiles to better reflect real operating conditions.
- Transport and delivery costs are excluded; it would be a good idea to investigate, especially, their impact on economic modelling.
- Different combinations of existing ESS technologies can be considered to improve the technical features of the HGSS and overall system; future studies should explore hybrid systems to reduce curtailed energy waste and improve utilisation.

5. Conclusions

The main contribution of this study lies in the development of a comprehensive modelling framework for power-to-gas hydrogen production based on CWE. The proposed model introduces a systematic approach to quantifying and utilising CWE for hydrogen generation, addressing the inherent intermittency and unpredictability of renewable power availability. The proposed approach is most applicable to locations characterised by persistent curtailment and viable hydrogen offtake pathways. It integrates detailed techno-economic models of the key subsystems, including the electrolyser, buffer tank, compressor, and main tank, to capture both dynamic performance and long-term financial outcomes. By linking real curtailment time-series data with hydrogen production, storage sizing, and cost evaluation, the model provides a robust tool for assessing system feasibility and optimisation under variable energy-input scenarios. It should also be noted that, in its present form, the framework is intended for a fixed hydrogen-demand case supplied by a single curtailed wind input. Accordingly, more complex scenarios, including multi-energy integration, variable hydrogen demand, and real-time market participation, would require further model development.

This work, therefore, contributes a novel method for representing CWE in hydrogen production planning. It offers new insights into the optimal design and operation of seasonal hydrogen storage systems. This study focuses on two key metrics, the LCOH and the NPV, which serve as crucial indicators of system performance and economic viability. The model designs were evaluated through sensitivity analysis, and LCOH was used to rank output plans. A multi-objective decision-making framework incorporating LCOH, NPV, present-value expenditure, and hydrogen demand met was employed to compare configurations and identify the optimal plan. The best-performing configuration corresponded to a curtailed wind input of 70.2 MWh, an electrolyser capacity of 2.3 MW, a main tank volume of 94 m^3, and a buffer tank of 75 m^3. This system achieved an LCOH of £3.51/kg and an NPV of £2.17 M and met 98.01% of hydrogen demand with a payback period of approximately 15 years. The proposed modelling framework and optimisation approach can be further applied to determine the optimal design capacities of similar systems using curtailed renewable energy, ensuring a balance between technical reliability and economic feasibility.

For context, the estimated LCOH obtained in this study (£3.51/kg) compares favourably with values reported for other green hydrogen production pathways. Recent techno-economic studies of grid-connected or renewable dedicated electrolysis typically report LCOH values in the range of approximately £3.2–£4.8/kg, depending on electrolyser utilisation, electricity pricing, and storage assumptions [12,15]. The comparatively lower LCOH achieved here is primarily attributable to the targeted utilisation of curtailed wind energy, combined with optimised electrolyser sizing and seasonal hydrogen storage, highlighting the economic potential of curtailment-driven power-to-gas systems.

Author Contributions: Conceptualisation, A.A.A.; methodology, A.A.A.; software, A.A.A.; validation, A.A.A., M.N. and D.T.G.; formal analysis, A.A.A.; investigation, A.A.A.; resources, D.T.G.; data curation, A.A.A.; writing original draft preparation, A.A.A.; writing review and editing, M.N. and D.T.G.; visualisation, A.A.A.; supervision, D.T.G.; project administration, D.T.G. All authors have read and agreed to the published version of the manuscript.

Funding: This research was funded by the Embassy of the Libyan Arab Republic in London.

Institutional Review Board Statement: Not applicable.

Informed Consent Statement: Not applicable.

Data Availability Statement: The data presented in this study are available from the corresponding author upon reasonable request.

Acknowledgments: The authors acknowledge the support of The University of Sheffield. If applicable, AI-assisted language polishing may be disclosed here, in accordance with journal policy.

Conflicts of Interest: The authors declare no conflicts of interest.

Abbreviations

AC	Alternating current
BESS	Battery energy storage system
BoL	Beginning of life
BoP	Balance of plant
CAPEX	Capital expenditure
CWE	Curtailed wind energy
DC	Direct current
EMS	Energy management system
EoL	End of life
ESS	Energy storage system
HGSS	Hydrogen generation and storage system
HPT	High-pressure tank
LCOH	Levelised cost of hydrogen
LHV	Lower heating value
LPT	Low-pressure tank
MAE	Mean absolute error
MAPE	Mean absolute percentage error
MHD	Met hydrogen demand
NPV	Net present value
OPEX	Operating expenditure
P2G	Power-to-gas
PEM	Polymer electrolyte membrane
RES	Renewable energy source
SOC	State of charge
UK	United Kingdom

Nomenclature

Acronyms	Symbols
$U(z)$	Wind speed at height z (m/s)
$U_{z,\mathrm{ref}}$	Wind speed at reference height z_{ref} (m/s)
z	Target height (m)
z_{ref}	Reference height (m)
z_0	Surface roughness length (m)
h	Wind turbine hub height (m)
$E_{\mathrm{HH,avg}}(t)$	Average curtailed energy over half-hour interval t (MWh)
N	Number of years
$E_y(t)$	Curtailed energy at time interval t (MWh)
$P_{\mathrm{wt}}(t)$	Wind turbine electrical power at time t (MW)
$P_{\mathrm{Inst,Cap}}$	Installed wind farm capacity (MW)
$P_{\mathrm{curt}}(t)$	Curtailed power at time t (MW)
$P_{\mathrm{curt,avg}}(t)$	Average curtailed power at time t (MW)
$P_{\mathrm{curt,norml}}(t)$	Normalised curtailed power at time t (–)
Δt	Time-step duration (s)
$\eta_{\mathrm{transformer}}$	Transformer efficiency (%)
$\eta_{\mathrm{AC\text{-}DC}}$	AC/DC rectifier efficiency (%)
$\eta_{\mathrm{DC\text{-}DC}}$	DC/DC converter efficiency (%)
η_{total}	Total conversion efficiency (%)
$P_{\mathrm{elr}}(t)$	Electrolyser input power at time t (kW)
$P_{\mathrm{elr,r}}$	Electrolyser power request (kW)
$P_{\mathrm{elr,d}}(t)$	Electrolyser power demand at time t (kW)
$P_{\mathrm{elr,min}}$	Minimum electrolyser power (kW)
$P_{\mathrm{elr,nom}}$	Nominal electrolyser power (kW)
$\dot{m}_{\mathrm{H_2}}(t)$	Hydrogen mass flow rate at time t (kg/h)
$\eta_{\mathrm{stack}}(t)$	Electrolyser stack efficiency at time t (kg H_2/kWh)
$\Delta P_{\mathrm{elr}}/\Delta t$	Electrolyser ramp rate (kW/s)
T_{startup}	Electrolyser startup time (s)
T_{shutdown}	Electrolyser shutdown time (s)
$R_{\mathrm{p,up}}$	Maximum positive ramp rate (W/s)
$R_{\mathrm{p,down}}$	Maximum negative ramp rate (W/s)
$E_{\mathrm{stack,l,p}}$	Stack energy consumption at low-power operation (kWh)
$E_{\mathrm{stack,r,p}}$	Stack energy consumption at rated-power operation (kWh)
$E_{\mathrm{stack,total}}$	Total stack energy consumption (kWh)
E_{Lifetime}	Lifetime energy consumption (kWh)
$P_{\mathrm{hgss,d}}(t)$	HGSS power demand at time t (kW)
$P_{\mathrm{hgss}}(t)$	Total HGSS power consumption at time t (kW)
P_{Pass}	Unused or pass-through curtailed power (MW)
$LHV_{\mathrm{H_2}}$	Lower heating value of hydrogen (kWh/kg)
P_{tk}	Tank internal pressure (bar)
V_{tk}	Tank volume (m^3)
T_{tank}	Tank temperature (K)
$P_{\mathrm{bar,tank}}$	Tank pressure (bar)
V_{tank}	Tank volume (m^3)
$M_{\mathrm{tk,rem}}(t)$	Remaining hydrogen mass in the tank at time t (kg)
$M_{\mathrm{tk,avg}}(t)$	Average hydrogen mass in the tank at time t (kg)
$\dot{m}_{\mathrm{tk,in,d}}(t)$	Hydrogen mass flow rate into the tank due to demand at time t (kg/h)
$\dot{m}_{\mathrm{tk,out,d}}(t)$	Hydrogen mass flow rate out of the tank due to demand at time t (kg/h)
$\dot{m}_{\mathrm{tk,in,max}}(t)$	Maximum hydrogen mass inflow rate to the tank at time t (kg/h)
$\dot{m}_{\mathrm{tk,out,max}}(t)$	Maximum hydrogen mass outflow rate from the tank at time t (kg/h)

https://doi.org/10.3390/en19092232

SOC_{tk}	Tank state of charge (%)
$SOC_{\mathrm{tk,max}}$	Maximum tank state of charge (%)
$SOC_{\mathrm{tk,min}}$	Minimum tank state of charge (%)
$SOC_{\mathrm{tk,inital,cap}}$	Initial tank state of charge (%)
SOC_{lpt}	Low-pressure tank state of charge at time t (%)
$SOC_{\mathrm{lpt,max}}$	Maximum low-pressure tank state of charge (%)
$SOC_{\mathrm{lpt,min}}$	Minimum low-pressure tank state of charge (%)
$SOC_{\mathrm{lpt,tr}}$	Low-pressure tank threshold state of charge (%)
$SOC_{\mathrm{lpt,tr2}}$	Minimum low-pressure tank threshold for reliable compressor operation (%)
SOC_{hpt}	High-pressure tank state of charge at time t (%)
$SOC_{\mathrm{hpt,max}}$	Maximum high-pressure tank state of charge (%)
$SOC_{\mathrm{hpt,tr}}$	High-pressure tank refill trigger threshold (%)
Δ_{lpt}	Low-pressure tank hysteresis margin (%)
Δ_{hpt}	High-pressure tank hysteresis margin (%)
$Tank_{\mathrm{noml,cap}}$	Nominal tank capacity (kg)
$\dot{m}_{\mathrm{comp,in}}(t)$	Hydrogen mass flow rate entering the compressor at time t (kg/h)
$\dot{m}_{\mathrm{comp,out}}(t)$	Hydrogen mass flow rate leaving the compressor at time t (kg/h)
$\dot{m}_{\mathrm{comp}}(t)$	Compressor hydrogen mass flow rate at time t (kg/h)
$\dot{m}_{\mathrm{comp,r}}$	Rated compressor hydrogen mass flow rate (kg/h)
$\dot{V}_{\mathrm{N}}$	Volumetric flow rate at normal conditions (Nm^3/h)
$\dot{V}_{\mathrm{s}}(t)$	Volumetric flow rate at suction conditions at time t (m^3/h)
$\dot{V}_{\mathrm{d}}(t)$	Volumetric flow rate at discharge conditions at time t (m^3/h)
P_{N}	Pressure at normal conditions (Pa)
T_{N}	Temperature at normal conditions (K)
$P_{\mathrm{s}}(t)$	Compressor suction pressure at time t (Pa)
$T_{\mathrm{s}}(t)$	Compressor suction temperature at time t (K)
$P_{\mathrm{d}}(t)$	Compressor discharge pressure at time t (Pa)
$T_{\mathrm{d}}(t)$	Compressor discharge temperature at time t (K)
$C_{\mathrm{comp}}(t)$	Compressor operating state or control signal at time t (–)
$P_{\mathrm{comp}}(t)$	Compressor power at time t (kW)
$P_{\mathrm{comp,d}}(t)$	Compressor power demand at time t (kW)
$q_{\mathrm{H_2O}}(t)$	Water flow rate at time t (L/h)
$k_{\mathrm{H_2O}}$	Water consumption per kg of hydrogen produced (L/kg)
$P_{\mathrm{pump}}(t)$	Pump power at time t (kW)
$P_{\mathrm{pump,d}}(t)$	Pump power demand at time t (kW)
γ	Specific weight of water ($\mathrm{N/m}^3$)
H	Pump hydraulic head (m)
η_{pump}	Pump efficiency (%)
$\mathrm{H_2O}$	Water
R	Universal gas constant (J/mol·K)
$M_{\mathrm{h_2}}$	Molar mass of hydrogen (kg/mol)
t	Time
$Sample_{\mathrm{rate}}$	Sampling rate (s^{-1})
$E_{\mathrm{pur},y}$	Annual electricity purchase cost (£)
$E_{\mathrm{total,pur}}$	Total electricity purchase cost (£)
$C_{\mathrm{H_2O,total}}$	Total water cost (£)
$Q_{\mathrm{H_2O,total}}$	Total water consumption (kg)
$C_{\mathrm{kg,H_2O}}$	Water cost per unit mass (£/kg)
C_{elr}	Electrolyser capital cost (£)
C_{ins}	Installation and civil works cost (£)
C_{inv}	Inverter cost (£)
$C_{\mathrm{stack,rep}}$	Stack replacement cost (£)

$Pur_{\mathrm{kW,elr}}$	Unit electrolyser cost (£/kW)
$C_{\mathrm{kW,ins}}$	Unit installation cost (£/kW)
$Pur_{\mathrm{kW,inv}}$	Unit inverter cost (£/kW)
$Pur_{\mathrm{kW,rep}}$	Unit stack replacement cost (£/kW)
$\mathrm{stack}_{\mathrm{rep,no}}$	Number of stack replacements (–)
C_{sto}	Storage system cost (£)
$Sto_{\mathrm{noml,cap}}$	Nominal storage capacity (kg)
$Pur_{\mathrm{kg,sto}}$	Unit storage cost (£/kg)
C_{comp}	Compressor cost (£)
$Pur_{\mathrm{kW,comp}}$	Unit compressor cost (£/kW)
$C_{\mathrm{sto,total}}$	Total storage-system cost (£)
$C_{\mathrm{hgss,total}}$	Total HGSS cost (£)
$CAPEX_{\mathrm{hgss}}$	HGSS capital expenditure (£)
$OPEX_{\mathrm{hgss}}$	HGSS operating expenditure (£/year)
$Rev_{\mathrm{H_2}}(t)$	Hydrogen sales revenue in year t (£)
PV_{Exp}	Present value of expenditure (£)
PV_{Rev}	Present value of revenue (£)
$\mathrm{H_2}(t)$	Annual hydrogen production in year t (kg)
r	Discount rate (%)
$Rev_{\mathrm{H_2}}$	Revenue from hydrogen sales (£)

References

1. Rozzi, E.; Minuto, F.D.; Lanzini, A. Dynamic modeling and thermal management of a Power-to-Power system with hydrogen storage in microporous adsorbent materials. *J. Energy Storage* **2021**, *41*, 102953.
2. Hawkes, B. GB Renewables Map: Curtailment. 2025. Available online: https://renewables-map.robinhawkes.com/curtailment (accessed on 28 April 2026).
3. Department for Energy Security and Net Zero. Digest of UK Energy Statistics (DUKES) 2024: Chapter 5—Electricity. 2024. Available online: https://www.gov.uk/government/statistics/digest-of-uk-energy-statistics-dukes-2024 (accessed on 1 February 2025).
4. Brouwer, A.S.; Van Den Broek, M.; Seebregts, A.; Faaij, A. Impacts of large-scale Intermittent Renewable Energy Sources on electricity systems, and how these can be modeled. *Renew. Sustain. Energy Rev.* **2014**, *33*, 443–466.
5. Asmelash, E.; Prakash, G.; Gorini, R.; Gielen, D. Role of IRENA for global transition to 100% renewable energy. In *Accelerating the Transition to a 100% Renewable Energy Era*; Springer: Berlin/Heidelberg, Germany, 2020; pp. 51–71.
6. Hosseini, S.E.; Butler, B.; Wahid, M.A. Hydrogen as a battery for a rooftop household solar power generation unit. *Int. J. Hydrogen Energy* **2020**, *45*, 25811–25826.
7. Nikolaos, P.C.; Marios, F.; Dimitris, K. A review of pumped hydro storage systems. *Energies* **2023**, *16*, 4516.
8. Rabi, A.M.; Radulovic, J.; Buick, J.M. Comprehensive review of compressed air energy storage (CAES) technologies. *Thermo* **2023**, *3*, 104–126.
9. Clegg, S.; Mancarella, P. Integrated modeling and assessment of the operational impact of power-to-gas (P2G) on electrical and gas transmission networks. *IEEE Trans. Sustain. Energy* **2015**, *6*, 1234–1244.
10. De Corato, A.M.; Dozein, M.G.; Riaz, S.; Mancarella, P. Hydrogen Electrolyzer Load Modelling for Steady-State Power System Studies. *IEEE Trans. Power Deliv.* **2023**, *38*, 4312–4323.
11. Clegg, S.; Mancarella, P. Storing renewables in the gas network: Modelling of power-to-gas seasonal storage flexibility in low-carbon power systems. *IET Gener. Transm. Distrib.* **2016**, *10*, 566–575.
12. Biggins, F.; Brown, S. Optimising onshore wind with energy storage considering curtailment. *Energy Rep.* **2022**, *8*, 34–40.
13. Yan, Y.; Wang, Y.; Yan, J.; Zhang, H.; Shang, W. Wind electricity-hydrogen-natural gas coupling: An integrated optimization approach for enhancing wind energy accommodation and carbon reduction. *Appl. Energy* **2024**, *369*, 123482.
14. Al-Mahmodi, M.; Ayadi, O.; Wang, Y.; Al-Halhouli, A. Sensitivity-based techno-economic assessment approach for electrolyzer integration with hybrid photovoltaic-wind plants for green hydrogen production. *Int. J. Hydrogen Energy* **2025**, *97*, 904–919.
15. Rezaei, M.; Akimov, A.; Gray, E.M.A. Techno-economics of offshore wind-based dynamic hydrogen production. *Appl. Energy* **2024**, *374*, 124030.
16. Jovan, D.J.; Pregelj, B.; Sekavčnik, M.; Dolanc, G. Sizing of a hydrogen system for green-hydrogen production by utilising surplus water accumulation in a hydropower plant. *Renew. Energy* **2025**, *255*, 123849.

17. Park, J.; Ryu, K.H.; Kim, C.H.; Cho, W.C.; Kim, M.; Lee, J.H.; Cho, H.S.; Lee, J.H. Green hydrogen to tackle the power curtailment: Meteorological data-based capacity factor and techno-economic analysis. *Appl. Energy* **2023**, *340*, 121016.
18. Abadie, L.M.; Chamorro, J.M. Investment in wind-based hydrogen production under economic and physical uncertainties. *Appl. Energy* **2023**, *337*, 120881.
19. Ferguson, J.L.; Robinson, A.; Crawford, S.; Mignard, D. Impact of integration of wind and tidal power on hydrogen production costs (March 2021). In Proceedings of the 14th European Wave and Tidal Energy Conference, Plymouth, UK, 5–9 September 2021; pp. 1–7. Available online: https://vb.nweurope.eu/media/15876/20210330-jf-ewtec-2021-paper-for-submission-emec.pdf (accessed on 17 May 2024).
20. Niaz, H.; Zarei, M.; Shams, M.H.; Won, W.; Liu, J.J. Curtailment to cashflow: Exploring BESS and hydrogen for renewable energy profitability. *J. Energy Storage* **2024**, *77*, 109990.
21. Zhao, G.; Nielsen, E.R.; Troncoso, E.; Hyde, K.; Romeo, J.S.; Diderich, M. Life cycle cost analysis: A case study of hydrogen energy application on the Orkney Islands. *Int. J. Hydrogen Energy* **2019**, *44*, 9517–9528.
22. Wind Turbine Models. Alstom ECO 122/2700. 2024. Available online: https://en.wind-turbine-models.com/turbines/629-alstom-eco-122-2700 (accessed on 30 April 2025).
23. Duffield, P.; de Berker, A. UK Wind Curtailment Monitor. n.d. Dashboard Showing UK Wind Power Discarded Due to Transmission Constraints Using Data from the Elexon Data Portal. Available online: https://zenodo.org/records/13936552 (accessed on 18 March 2024).
24. H2planet. Horizon VL II-M 100. Available online: https://www.h2planet.eu/en/detail/horizon_vl100l (accessed on 10 January 2024).
25. Aminaho, E.N.; Aminaho, N.S.; Aminaho, F. Techno-economic assessments of electrolyzers for hydrogen production. *Appl. Energy* **2025**, *399*, 126515.
26. Shaner, M.R.; Atwater, H.A.; Lewis, N.S.; McFarland, E.W. A comparative technoeconomic analysis of renewable hydrogen production using solar energy. *Energy Environ. Sci.* **2016**, *9*, 2354–2371.
27. Hyde, K.; Ellis, A.; Power, I. *Feasibility of Hydrogen Bunkering*; ITM Power: Sheffield, UK, 2019.
28. ITM Power. *Final Results Presentation*; ITM Power: Sheffield, UK, 2016.
29. Giner, Inc. Webpage: High Pressure Hydrogen Generators. 2016. Available online: http://www.ginerinc.com/ (accessed on 12 December 2024).
30. Hydrogenics. Renewable Hydrogen Solutions. 2016. Available online: https://www.hydrogenics.com/wp-content/uploads/HYDROGENICS_RenewableHydrogen.pdf (accessed on 18 March 2024).
31. Siemens AG. SILYZER 200: PEM Electrolysis System. 2024. Available online: https://www.industry.siemens.com/topics/global/en/pem-electrolyzer/silyzer/Documents/silyzer-200-en_v1.3_InternetVersion.pdf (accessed on 13 February 2024).
32. Gemmer-Berkbilek, K. Field Test Experience with Areva's PEM Electrolysis Systems. In *Technologieentwicklung PTDT-G*; Areva Gmbh: Erlangen, Germany, 2016.
33. OnSite, Proton. M-Series PEM Electrolyzer: Scalable, MW-Class Hydrogen Generation Systems [Brochure Rev C]. 2016. Available online: https://www.silpac.com.cn/download/M-Series-Containerized-Spec-Sheet-Rev-A.pdf (accessed on 20 August 2024).
34. Buttler, A.; Spliethoff, H. Current status of water electrolysis for energy storage, grid balancing and sector coupling via power-to-gas and power-to-liquids: A review. *Renew. Sustain. Energy Rev.* **2018**, *82*, 2440–2454.
35. Angstrom Advanced Inc. Webpage. 2024. Available online: http://www.angstrom-advanced.com/ (accessed on 10 May 2024).
36. Kobelco Eco-Solutions Co., Ltd. High-Purity Hydrogen Oxygen Generator HHOG: Product Catalog. 2024. Available online: https://www.kobelco-eco.co.jp/product/pdf/hhog/hhog_catalog_english.pdf (accessed on 28 April 2026).
37. Green Hydrogen Systems. HyProvide X-Series: 6 MW Modular Electrolyser. Available online: https://www.greenhydrogensystems.com/electrolysers/hyprovide-x-series-6mw-modular-electrolyser (accessed on 27 April 2026).
38. Sylatech GmbH. Company Webpage. 2016. Available online: http://www.sylatech.de/ (accessed on 19 May 2024).
39. International Energy Agency. *The Future of Hydrogen*; IEA: Paris, France, 2019. Available online: https://www.iea.org/reports/the-future-of-hydrogen (accessed on 8 April 2024).
40. Reddi, K.; Elgowainy, A.; Rustagi, N.; Gupta, E. Two-tier pressure consolidation operation method for hydrogen refueling station cost reduction. *Int. J. Hydrogen Energy* **2018**, *43*, 2919–2929.
41. Fragiacomo, P.; Genovese, M. Developing a mathematical tool for hydrogen production, compression and storage. *Int. J. Hydrogen Energy* **2020**, *45*, 17685–17701.
42. Atherton, J.; Xie, W.; Farazi, F.; Mosbach, S.; Akroyd, J.; Kraft, M. *Breakdown of British wind Curtailment Using a Multi-Source Knowledge Graph Approach*; Cambridge Centre for Computational Chemical Engineering: Cambridge, UK, 2023.

43. Statistics How to. Absolute Error and Mean Absolute Error. 2016. Available online: https://www.statisticshowto.com/absolute-error/ (accessed on 12 April 2026).
44. To, Statistics How. Mean Absolute Percentage Error. 2020. Available online: https://www.statisticshowto.com/mean-absolute-percentage-error-mape/ (accessed on 12 April 2026).